DEUTSCHES ELEKTRONEN-SYNCHROTRON DESY

DESY 80/121
December 1980

# SCALAR VS. VECTOR GLUONS IN INCLUSIVE $\gamma$-DECAYS OF HEAVY $1^{--}$ QUARKONIUM: RATES, SPECTRA, ANGULAR CORRELATIONS AND PHOTON POLARIZATIONS

by

J. G. Körner
*Deutsches Elektronen-Synchrotron DESY, Hamburg*

D. McKay
*II. Institut für Theoretische Physik der Universität Hamburg*

NOTKESTRASSE 85 · 2 HAMBURG 52

To be sure that your preprints are promptly included in the
HIGH ENERGY PHYSICS INDEX ,
send them to the following address ( if possible by air mail ) :

DESY
Bibliothek
Notkestrasse 85
2 Hamburg 52
Germany

DESY 80/121
December 1980

# Scalar vs. Vector Gluons in Inclusive $\gamma$-Decays of Heavy $1^{--}$ Quarkonium: Rates, Spectra, Angular Correlations and Photon Polarizations

J. G. Körner

Deutsches Elektronen-Synchrotron DESY, Hamburg

D. McKay

II. Institut für Theoretische Physik der Universität Hamburg *

Abstract

We calculate the decay of a heavy $1^{--}$ quarkonium state into a photon and 2 vector or scalar gluons in Born approximation. We find significant and testable differences in the predictions of the two theories for the $\gamma$-inclusive rates, the photon energy spectrum, the angular correlations between the $\gamma$-event plane and the beam direction and for the linear polarization of the produced photon.

* Alexander von Humboldt fellow on leave from the University of Kansas, Lawrence, Kansas, U.S.A.



## I. Introduction

The $\gamma$-inclusive decays of heavy $J^{PC} = 1^{--}$ quarkonium states constitute an important test of perturbative QCD (quantum chromodynamics), which predicts that these decays proceed by $1\gamma + 2$ gluon emission [1,2,3]. DORIS data [4] already support the QCD 3-gluon origin of the purely hadronic decays of $\Upsilon(9.46)$, and PETRA data [5,6] at higher energies beautifully confirm the QCD predictions on the $q+\bar{q}$+gluon origin of hadronic jets. The $\gamma$-inclusive decays of $1^{--}$ charmonium states are quite a clean and independent check of the QCD theory.

Measurement of inclusive, direct photon decays of the $J/\psi$ show roughly the rate expected in QCD [7,8]. In one experiment [7], the photon spectrum is much softer than that expected from the QCD calculation. The second experiment [8] shows a harder spectrum, not inconsistent with QCD. Apart from the experimental discrepancy, the relatively low energy per decay-gluon which is available at the $J/\psi$ mass makes suspect the application of perturbative QCD to the decay of $J/\psi$. The structure observed in $J/\psi \to \gamma + X$ and $\psi' \to \gamma + X$ [9] gamma-energy spectra also indicate that the Born term cannot be the whole story in the $J/\psi$ region. Since one expects the perturbative QCD predictions to be more reliable at higher gluon energies, the prospects of significant increases in $\Upsilon$-data from CESR and DORIS and possibly VEPP 4 in the next few years encourage us to review and extend the calculations of $\gamma$-inclusive decays of quarkonium. The disadvantage in rate of $\gamma$-inclusive decays (the branching ratio should be roughly 1/4 that of the corresponding $\psi/J$ inclusive-$\gamma$ branching ratio, or about 2 %) is compensated for by the obvious advantage that the photon's energy and direction can be measured and directly be used in the analysis of the process. The corresponding analysis of the

three gluon process will always involve uncertainties related to the non-perturbative fragmentation process of the gluons.

Since the quarkonium is produced in a polarized state in $e^+e^-$ interactions, there will be correlations between the decay plane and the beam axis which provide important tests of the dynamics of the decay process. The well-defined orientation of the $\gamma$-inclusive event allows one to measure and test these correlation predictions. The (four) correlation coefficients calculated via QCD turn out to be of roughly the same magnitude in this process, and beam-event correlations are correspondingly strong.

Beam-event correlation measurements have also been suggested for the $q+\bar{q}+$gluon final state of $e^+e^-$-annihilation [10]. However, these measurements are more difficult to perform for two reasons. First, the correlations are dominated by the transverse helicity cross-section $\sigma_u$ because it is the most singular in the soft/collinear gluon limit. Consequently the correlations predominantly show the structure of the underlying Born-term process $e^+e^- \to q\bar{q}$ and additional correlations are hard to detect. Second, there are only few events with a well developed plane structure - again for the reason that the cross section is so strongly peaked towards the soft/collinear two jet region. These disadvantages do not exist in the $Q\bar{Q} \to gg\gamma$ process, and we feel that this process offers the best chance of measuring such correlations.

Photon polarization measurements, should they prove feasible, would enlarge the number of testable coefficients. Just the total polarization asymmetry measurement would yield valuable information about the mechanism which underlies quarkonium decay.



In the derivation of cross-sections and correlation coefficients, we use the helicity formalism throughout. This method has considerable technical advantage in these calculations. Since its application to quarkonium decay is new, we exhibit some intermediate steps. Results for colored, scalar gluon amplitudes are also derived in every case, and several comparisons with QCD are made.

In the next section we write down the matrix elements for the vector case and give helicity amplitudes and the helicity structure functions (cross-sections) $\sigma_u$, $\sigma_L$, $\sigma_T$ and $\sigma_I$ which appear in the rate formula. Differential and integrated rates are given. In Sec. 3 we present our results for the rates, spectra, integrated helicity structure functions, average opening angle between gluon jets, polar angle distributions, average thrust and polarization asymmetries. We comment on the feasibility of polarization measurements. An appendix contains the outline of the helicity formalism applied to the scalar gluon case, and detailed formulas are tabulated there and referred to in the figures and remarks in the main text.

## II. Matrix Elements and Helicity Amplitudes

The calculation of the decay of a heavy quarkonium state into a photon and two vector gluons proceeds in complete analogy to the corresponding positronium decay calculation. Figure 1 illustrates the process. In the nonrelativistic approximation, and neglecting binding energies, one has $M \cong 2m$ and $P = p - \bar{p} \cong 2p$, where M and m are the masses of the quarkonium state and its heavy quark constituent, respectively. For the spin projection of the quarkonium state, it is convenient to use the covariant form $\not{\epsilon}(\not{P}-M) = 2\not{\epsilon}(\not{p} - m)$, which is well known from relativistic SU(6) calculations [11]. The amplitude is then given

by the covariant trace

$$M_{ij} = N_{ij}\{2m\,\mathrm{Tr}[\not\epsilon(\not p - m)\not\epsilon_3^*(-\not p+\not p_3 - m)^{-1}\not\epsilon_2^*(\not p - \not p_1 - m)^{-1}\not\epsilon_1^*] + \text{cyclic perm. } (1,2,3)\} \quad (1)$$

All constants have been absorbed into $N_{ij} = N\delta_{ij}$, where i,j are color indices and

$$N = 2\sqrt{2}\,\sqrt{\alpha}\,\alpha_s(4\pi)^{3/2} e_Q\,\psi(0)/\sqrt{3}\,m^{3/2}$$

$\psi(0)$ is the wave function evaluated at the origin, $e_Q$ is the charge of the heavy quark, and $\alpha$ and $\alpha_s$ are the electromagnetic and strong coupling constants, respectively. Decay rates are computed according to the rules for a massive spin one boson decaying into three massless bosons with the normalization indicated above.

After performing the trace calculation, the amplitude (1) can be arranged into the convenient form [12]

$$\begin{aligned} M_{ij} = -2N_{ij}\frac{m^4}{x_1x_2x_3}\{&(e_1^*\cdot e_2^*)[-(p_1\cdot p_3)(p_2\cdot e_3^*)(p_1\cdot e) - (p_1\cdot p_3)(p_2\cdot p_3)(e_3^*\cdot e) \\ &-(p_2\cdot p_3)(p_1\cdot e_3^*)(p_2\cdot e)] + (e\cdot e_3^*)[(p_1\cdot p_3)(p_2\cdot e_1^*)(p_3\cdot e_2^*) \\ &-(p_1\cdot p_2)(p_3\cdot e_1^*)(p_3\cdot e_2^*) + (p_2\cdot p_3)(p_1\cdot e_2^*)(p_3\cdot e_1^*)] \\ &+ (1\leftrightarrow 3) + (2\leftrightarrow 3)\} \end{aligned} \quad (2)$$

We have used the conventional scaled energies $x_i = E_i/m$, so that $x_1+x_2+x_3 = 2$. Useful formulas are: $p\cdot p_i = m^2x_i$, $p_i\cdot p_j = 2m^2(1-x_k)$ where $i \neq j \neq k$, and



$(P - p_i)^2 - m^2 = 2m^2x_i$ which occur in the propagator denominators.

In the usual approach, cross sections are derived from Eq. (2) by squaring and summing over spins. We shall instead calculate helicity amplitudes first and then obtain cross sections by evaluating the appropriate sums of bilinear forms of helicity amplitudes. One can extract all needed physics information directly from the bilinears of helicity amplitudes, which have simple forms. This procedure is shorter and more transparent than the usual one of squaring and summing on spins - especially in the cases where polarization projections are necessary.

Our event coordinate system is fixed according to Fig. 2. The z-direction points along the photon momentum and the x-axis is in the half plane of the higher momentum gluon. Momenta are $p_1 = E_1(1;001)$, $p_2 = E_2(1;\sin\theta_{12},0,\cos\theta_{12})$, $p_3 = E_3(1;-\sin\theta_{13},0,\cos\theta_{13})$ and polarization vectors are (1 = photon and 2,3 = gluons)

$$e_1^{*\pm} = \frac{1}{\sqrt{2}}(0;\mp1,-1,0), \quad e_2^{*\pm} = \frac{1}{\sqrt{2}}(0;\cos\theta_{12},-1,\mp\sin\theta_{12})$$

$$e_3^{*\pm} = \frac{1}{\sqrt{2}}(0;\mp\cos\theta_{13},-i,\mp\sin\theta_{13}),\ e^{\mp} = \mp\frac{1}{\sqrt{2}}(0;1,\mp i,0) \text{ and } e^{o} = (0;0,0,1)$$

Here $\theta_{ij}$ is the angle between particles i and j. From spin counting, one finds that there are twelve independent helicity amplitudes, designated $H_{\lambda_1\lambda_2\lambda_3;\,\lambda_{Q\bar{Q}}}$ as follows:

Transverse $Q\bar{Q}$ polarization

$$H_{+++;+} = 0$$

$$H_{++-;+} = (1-x_2)(1-x_3)$$

$$H_{+-+;+} = (1-x_2)(1-x_3)$$

$$H_{+--;+} = (1-x_1)x_1^2 \qquad \otimes \text{common } \tfrac{1}{2}N_{ij} \cdot \frac{1}{x_1^2 x_2 x_3} \text{ factor}$$

$$H_{-++;+} = 0$$

$$H_{-+-;+} = (1-x_1)(1-x_2)^2$$

$$H_{--+;+} = (1-x_1)(1-x_3)^2$$

$$H_{---;+} = 0 \qquad (3a)$$

Longitudinal $Q\bar{Q}$ polarization

$$H_{+++;o} = 0$$

$$H_{++-;o} = (1-x_3)X^{1/2} \qquad \otimes \text{common } \tfrac{1}{2}N_{ij} \frac{1}{x_1^2 x_2 x_3}$$

$$H_{+-+;o} = -(1-x_2)X^{1/2}$$

$$H_{-++;o} = 0$$

where $X = (1-x_1)(1-x_2)(1-x_3)$.

The remaining twelve helicity amplitudes can be obtained from the parity conditions

$$H_{-\lambda_1,-\lambda_2,-\lambda_3;-} = H_{\lambda_1,\lambda_2,\lambda_3;+}$$

$$H_{-\lambda_1,-\lambda_2,-\lambda_3;o} = -H_{\lambda_1,\lambda_2,\lambda_3;o} \qquad (3b)$$



Since the initial spin-one quarkonium is produced in a polarized state in $e^+e^-$-annihilation, beam-event correlations allow one to measure four decay structure functions, also loosely referred to as cross-sections, which are denoted by $\sigma_u$, $\sigma_L$, $\sigma_T$ and $\sigma_I$. The distribution is written as

$$\frac{d\Gamma}{dx_1 dx_2 d\chi d\cos\theta} = \frac{m}{8(4\pi)^4}\left[\sigma_u(1+\cos^2\theta) + 2\sigma_L \sin^2\theta + 2\sigma_T \sin^2\theta\cos 2\chi - 2\sqrt{2}\,\sigma_I \sin 2\theta\cos\chi\right] \qquad (4)$$

The polar angle $\theta$ and azimuthal angle $\chi$ are defined as drawn in Fig. 2. Measurements of $\sigma_u$, $\sigma_L$ and $\sigma_T$ do not require energy ordering of the two gluons, but only require that the event plane be determined. Measurement of $\sigma_I$ requires that gluon jet energies be measured and ordered. The reason for this difference between measurement of $\sigma_I$ and measurement of $\sigma_u$, $\sigma_L$ or $\sigma_T$ is seen as follows. When, as in QCD, the particles 2 and 3 are identical, then the coefficients $\sigma_u$, $\sigma_L$ and $\sigma_T$ are symmetric in exchange of $x_2$ and $x_3$. $\sigma_I$ is antisymmetric in $x_2$ and $x_3$. For an arbitrary $\chi$ value, the first three terms in (4) obtain equal contributions from points $(x_2,x_3)$ and points $(x_3,x_2)$, whereas the last term obtains cancelling contributions. But if the choice of $\chi$ is correlated with the energy identification (x-axis as in Fig. 2 in the half plane of the more energetic jet), then the $\cos\chi$ coefficient always has the same sign, and a non-trivial distribution results.

Now the four cross-sections in (4) can be expressed in terms of the helicity amplitudes of (3) by the relations

$$\sigma_u = 2 \sum_{\lambda_i} | H_{\lambda_1\lambda_2\lambda_3;+} |^2$$

$$\sigma_L = \sum_{\lambda_i} | H_{\lambda_1\lambda_2\lambda_3;0} |^2 \qquad (5)$$

$$\sigma_T = Re \sum_{\lambda_i} H_{\lambda_1\lambda_2\lambda_3;+} H^*_{\lambda_1\lambda_2\lambda_3;-}$$

$$\sigma_I = Re \sum_{\lambda_i} H_{\lambda_1\lambda_2\lambda_3;+} H^*_{\lambda_1\lambda_2\lambda_3;0}$$

where color summing has not been explicitly displayed in (5).

Since $\sigma_I$ does require energy ordering $x_2 > x_3$ in its measurement, we assume energy ordering to be done in the whole differential rate (4) and therefore include no 1/2 factor appropriate to identical gluons when all of phase space is integrated over. As remarked above, energy ordering is not necessary for $\sigma_u$, $\sigma_L$ and $\sigma_T$ which are correspondingly $x_2 \leftrightarrow x_3$ symmetric, as seen in Table I.

Armed with expressions (3) and (5), it is now an easy matter to calculate the cross-sections $\sigma_u$, $\sigma_L$, $\sigma_T$ and $\sigma_I$. We display these double differential quantities, which should be designated, e.g., $\sigma_u(x_1,x_2)$, in Table I. As in the formulas (4) and (5), we suppress the arguments for compactness of notation.

We have listed the total differential decay cross-section $\sigma = \sigma_u + \sigma_L$ in Table I instead of $\sigma_u$, since $\sigma$ takes the simple form which is well known from the positronium calculation of Ore and Powell [13]. Note that $\sigma_T$ and $\sigma_I$



need not be positive definite since they are interference terms.

The cross-sections $\sigma_i$ in Table I correspond to measurements where the polarization of the photon goes undetected, i.e. they are the sum $\sigma_i^{\parallel} + \sigma_i^{\perp}$, where $\sigma_i^{\parallel}$ and $\sigma_i^{\perp}$ are the corresponding rates with the photon being linearly polarized parallel and perpendicular, respectively, to the three-body event plane. The degree of linear polarization of the produced photon is given by the polarization asymmetry $A = (\sigma^{\parallel} - \sigma^{\perp})/(\sigma^{\parallel} + \sigma^{\perp})$. These quantities can also be calculated easily from the helicity amplitudes. One has

$$\sigma_u^{\parallel} - \sigma_u^{\perp} = -4 \sum_{\lambda} Re[(H_{+\lambda_2\lambda_3;+})(H^*_{-\lambda_2\lambda_3;+})]$$

$$\sigma_L^{\parallel} - \sigma_L^{\perp} = -2 \sum_{\lambda} (H_{+\lambda_2\lambda_3;0})(H^*_{-\lambda_2\lambda_3;0})$$

$$\sigma_T^{\parallel} - \sigma_T^{\perp} = -\sum_{\lambda} [(H_{+\lambda_2\lambda_3;+} H^*_{-\lambda_2\lambda_3;-}) + (H_{+\lambda_2\lambda_3;-} H^*_{-\lambda_2\lambda_3;+})]$$

$$\sigma_I^{\parallel} - \sigma_I^{\perp} = -\sum_{\lambda} [(H_{+\lambda_2\lambda_3;+})(H^*_{-\lambda_2\lambda_3;0}) + (H_{+\lambda_2\lambda_3;0})(H^*_{-\lambda_2\lambda_3;+})]$$

The differential distribution for the cross section difference in- and out-of-the production plane is the same as given in Eq.(4). In Appendix B we discuss an additional independent polarization contribution due to linear polarization in the x-y plane. This additional contribution does not, however, enter into the polar angle polarization distributions considered in this paper.

In the following we shall sometimes use the abbreviations $\sigma_i^{\pm} = \sigma_i^{\parallel} \pm \sigma_i^{\perp}$ where $\sigma_i^{+} \equiv \sigma_i$. The QCD expressions for these photon polarization-sensitive quantities are shown in Table II, where again the $x_1$ and $x_2$ arguments of the $\sigma_i$ are suppressed. The scalar gluon model predictions for the eight observables listed in Tables I and II are presented in the Appendix.

## III. Results

In this section we accumulate results of our calculations. We discuss in turn the expected rates of charmonium decay to $\gamma gg$ compared to $ggg$ in the vector and scalar gluon cases, the Dalitz plots and photon energy spectra which one expects, the polar beam-event correlation coefficient $\alpha(x_1)$, the average cosine of the opening angle between gluons, and the photon polarization asymmetry as it varies within the Dalitz plot boundaries, as it varies as a function of the photon momentum alone, and as it varies with photon angle. In addition, average gluon thrust is computed as a function of $x_1$, and also averaged over $x_1$.

(a) Rates: The lowest order QCD rate prediction is quite simple [1,2] and is obtained by comparing the graph of Fig. 1 with the corresponding one where the photon is replaced by a gluon. One finds

$$R_\gamma = \frac{\Gamma(Q\bar{Q} \to \gamma gg)}{\Gamma(Q\bar{Q} \to ggg)} = \frac{36}{5} \frac{\alpha}{\alpha_s} e_Q^2 \qquad (6)$$

where $\alpha$ is the electromagnetic fine-structure constant and $\alpha_s$ is the corresponding strong interaction constant and where $e_Q$ is the quark charge in units of e. The Lena collaboration at DESY [14] quotes a value $\alpha_s(M_\Upsilon^2) = 0.16 \,^{+0.04}_{-0.02} \pm 0.01$ from their analysis of $\Upsilon$ total width and leptonic branching ratios. With a b-quark charge of $e_Q = -1/3$, one estimates

$$R \cong 0.38 \,^{-.009}_{+.005} . \qquad (7)$$



The corresponding ratio in the scalar gluon case is complicated by the presence of infrared singularities. These singularities result from taking the quarks real rather than virtual and neglecting binding of quarks within the quarkonium [15].

The perturbative on-mass-shell treatment of the decay process will therefore be no longer reliable for small gluon energies. One must therefore introduce a cut-off on the gluon energy which may be reasonably estimated to be of the order of the binding energy in the quarkonium state. We quote the value of the ratio $R_\gamma$ as a function of the cutoff,

$$R_\gamma = \frac{16}{3} \frac{\alpha}{\bar{\alpha}_s} (e_Q)^2 \cdot \frac{I^{gg\gamma}(\Delta)}{I^{ggg}(\Delta)} = \frac{e_Q^2}{\bar{\alpha}_s} \cdot (0.39) \frac{I^{gg\gamma}(\Delta)}{I^{ggg}(\Delta)} \qquad (8)$$

where $\bar{\alpha}_s$ is the scalar gluon coupling constant, the functions $I^{gg\gamma}(\Delta)$ and $I^{ggg}(\Delta)$ are defined in Eqs. (A.4) and (A.5) of the Appendix. The range of the final, divergent $x_1$ integration is cut off at $x = \Delta$ below and $1-\Delta$ above, since the ggg amplitude blows up in the $x \to 0$ and $x \to 1$ limits. Taking several cut-off values we find

$$\begin{aligned} I^{gg\gamma}/I^{ggg} &= 1.00 \quad \Delta = 0.0 \\ " &= 1.42 \quad \Delta = 0.01 \\ " &= 2.09 \quad \Delta = .05 \\ " &= 2.28 \quad \Delta = 0.10 \\ " &= 2.38 \quad \Delta = 0.20 , \end{aligned} \qquad (9)$$

for a variation of about a factor two over these $\Delta$ values. For a rough estimate, this cutoff dependence poses no problem. As examples, we take the

value $I^{gg\gamma}/I^{ggg} = 2.28$ at $\Delta = 0.10$, and we take two different values of $\bar{\alpha}_s$ which have been quoted in recent experimental analyses. The (bad) fit value $\bar{\alpha}_s = 0.77$ by the PLUTO group [16] gives $R_\gamma \cong .08$, which is about twice as large as the estimate, Eq. (7), for the vector gluon case. *) The TASSO value [17] $\bar{\alpha}_s = 1.6$ (also poor confidence level) leads to $R_\gamma \cong 0.04$.

(b) Dalitz plot distributions and energy spectra: Turning next to the question of the spectra of the final state in $\gamma gg$ decay of quarkonium, we show the double differential decay rate summed over all spins in Fig. 3a. The formula is listed in Table I. The distribution has the rather uniform appearance already displayed by Koller and Walsh [2] for $gg\gamma$ and for the ggg case of a totally hadronic final state. The corresponding scalar gluon distribution is shown in Fig. 3b for comparison, and the strong spin dependence is immediately obvious. The scalar distribution formula is listed in the Appendix, Table A.I.

The remarks of Walsh and Zerwas [19] and Koller and Krasemann [18] concerning the three gluon case are appropriate here. They pointed out that the soft scalar gluon region is infrared singular because of the lack of spin-flip suppression of the pole in the quark propagator in the limit of a zero momentum gluon. As discussed above, the singularity is a theoretical artifact, a result of treating the quarks as on shell. The binding energy provides a very rough estimate of how far off shell the bound quark is, though the ratio of $gg\gamma$ and ggg rate

*) However, it has been argued by Koller and Krasemann [18] [Phys. Lett. 88B (1979) 119], by Walsh and Zerwas [19] [ibid. 93B (1980), 53] that the scalar gluon event shape is inconsistent with the data on $\Upsilon$ decay to hadrons.



is not very sensitive to the precise value as indicated in our discussion in connection with Eqs. (8) and (9). We choose $x = 0.9$, or $\Delta = 0.1$, as a cutoff in normalizing and displaying spectra in the photon energy variable, $x_1$. As in the case of three gluon final states, [18,19] the enhancement of decay probability when one scalar gluon is soft leads to an event configuration which is more like two jets than like three jets. The photon recoils against one gluon, the other gluon playing little role.

This two-jet-like feature of the scalar case is shown in another way by the comparison of the QCD $x_1$-spectrum and the scalar gluon spectrum in Fig. 4. The scalar spectrum is very hard, rising sharply above the QCD spectrum at an $x_1$ value of about 0.7. The spectra shown are both normalized to 1 in the interval $[0,0.9]$. The QCD spectrum is almost linear in $x_1$ (as in a $\gamma$ + 2 jets phase space model), deviating slightly from linearity near $x_1 = 1$. In Fig. 5 we show the corresponding thrust distributions, normalized to 1 in the thrust interval $[2/3, 0.9]$. Again the QCD case shows an almost linear dependence on thrust, whereas the scalar gluon case has the more peaked behaviour characteristic of the infrared singularity as $T \to 1$.

The beam-event correlation Eq. (4), when summed over photon and gluon spins and integrated over gluon energies, contains the four independent cross-sections, or structure functions, shown in Table III for the QCD case and in Table A.II of the Appendix for the scalar case. These cross-sections are plotted in Figures 6a and 6b, respectively.

One notes from Fig. 6a that the helicity cross-sections for the QCD-case are of comparable magnitude, whereas for scalar gluons $\sigma_u$ dominates over $\sigma_\ell, \sigma_T$

and $\sigma_T$ over most of the $x_1$-range. The dominance of $\sigma_u$ in the scalar gluon case results from its infrared singular nature as $x_1 \to 1$, just as in the QCD $q\bar{q}g$ situation [10]. The QCD results, shown in Fig. 6a, encourage one to expect that the correlation cross-sections $\sigma_u$, $\sigma_T$ and $\sigma_L$ can be individually measured, since photon momentum and the event plane are the only essential information needed.

(c) The polar correlation parameter

In Fig. 7 is shown a plot of the value of $\alpha$, the photon angular distribution parameter, as a function of $x_1$, the scaled photon energy [2]. $\alpha$ measures the decay of quarkonium into $\gamma$ + two gluons as a function of the angle between the photon direction and the $e^+e^-$ beam direction,

$$d\sigma/d\cos\theta \sim 1 + \alpha\cos^2\theta \quad \text{where} \quad \alpha = (\sigma_u - 2\sigma_L)/(\sigma_u + 2\sigma_L) \quad \text{and}$$

$\sigma_u$ and $\sigma_L$ are proportional to the probabilities that the decaying quarkonium state is transversely or longitudinally polarized in the photon direction, respectively. QCD predicts a distinctively sharp variation in the region $0.5 \lesssim x_1 \lesssim 1$ which should be testable and is certainly distinct from the scalar gluon case for which $\alpha$ is essentially 1 over the whole range due to the dominance of $\sigma_u$.

That $\alpha \to 1$ as $x_1 \to 1$ in both cases follows from the spin constraints on back-to-back particles with J = 1 whose $s_z$ projection along their colinear line of motion is necessarily $\pm$ 1. The distribution for decay of a state with J = 1 and $J_{z'} = \pm 1$ (z' = beam direction) into a state with J = 1 and $J_z = \pm 1$ along a new z direction at angle $\theta$ with respect to z' (z is the photon direction), is just $1 + \cos^2\theta$, or $\alpha = 1$ and $\sigma_L = 0$.



Choosing the z-axis along the photon's momentum is particularly well suited for seeing the distinctive QCD behavior in the polar angle distribution as compared to the scalar gluon case. If one uses the normal to the event plane to analyze the polar angle distributions, one obtains almost identical, flat distributions in both cases. To see this, transform the helicity cross-sections to a system where the normal to the event plane is the z-axis (transversity frame). One has in the new system [2]

$$\hat{\sigma}_u = \tfrac{1}{2}\sigma_u + \sigma_L - \sigma_T$$
$$\hat{\sigma}_L = \tfrac{1}{2}\sigma_u + \sigma_T \qquad (10)$$

and consequently

$$\hat{\alpha} = (\hat{\sigma}_u - 2\hat{\sigma}_L)/(\hat{\sigma}_u + 2\hat{\sigma}_L)$$
$$= -\tfrac{1}{3}(\sigma_u - 2\sigma_L + 6\sigma_T)/(\sigma_u + \tfrac{3}{2}\sigma_L + \tfrac{3}{2}\sigma_T).$$

For QCD one has $\hat{\alpha} = -1/3$ since $\sigma_L = 2\sigma_T$ (see Table 1) and thus no $x_1$-dependence of $\hat{\alpha}$. For scalar gluons one finds again $\hat{\alpha} \cong -1/3$ for $x_1 \to 1$ due to the dominance of $\sigma_u$ in the infrared limit. For smaller $x_1$-values, $\hat{\alpha}$ will become more negative. For example, one has $\hat{\alpha}(0) = -0.60$ and $\hat{\alpha}(0.5) = -0.47$.

In Fig. 8a we have plotted the QCD average values of $\alpha$, polarization asymmetry A and "grand average" thrust $\langle\langle T \rangle\rangle$, where the averages are taken in the interval $[x_1^c, 1]$. In Fig. 8b we have plotted the corresponding averages taken in the interval $[x_1^c, 0.9]$ for the scalar gluon case. We have displayed the dependence of the averages on the lower cutoff $x_1^c$ because low momentum photons are difficult to distinguish from background experimentally, and experimental

data will generally only be available above some $x_1^c > 0$ which depends on the particular detector. Published data are limited to $x_1^c \gtrsim 0.5$, [8,9] for example.

We avoided $x_1 = 1$ in the scalar gluon case because the infrared singularity in the model calculation at $x_1 = 1$ drives the averages to their value at $x_1 = 1$, for example $\langle \alpha \rangle = \alpha(1) = 1$, regardless of the lower integration limit $x_1^c$. Thus we define

$$\langle \alpha \rangle \equiv \frac{\int_{x_1^c}^{x_1^u} \alpha(x_1)\sigma(x_1)dx_1}{\int_{x_1^c}^{x_1^u} \sigma(x_1)dx_1}$$

and where $x_1^u = 1$ or 0.9 for QCD or scalar gluons, respectively. The plots show vividly that there is a big difference between the scalar gluon model predictions and those of QCD for the energy-averaged photon angular correlation. This difference persists in every averaging range except for $x_1^c$ very close to 1.

We continue our discussion by turning to the predictions for the average of the cosine of the opening angle between gluons and then return to Figs. 8a and 8b for remarks on "grand average" thrust and average polarization asymmetry.

(d) Average opening angle

In the average opening angle between the gluon jets $\langle \cos\theta_{23} \rangle$, an



interesting difference between the vector gluon case and the scalar gluon case developes as $x_1 \to 1$. $\langle \cos\theta_{23} \rangle$ is shown in Fig. 9, where one sees the expected back-to-back gluon configuration, $\langle \cos\theta_{23} \rangle \simeq -1$, for small photon momentum in both the scalar and vector gluon cases. But the singularity in the cross-section for the scalar case in the $x_1 \to 1$ limit gives such strong weight to the emission of a soft gluon, whose direction is unconstrained while the other gluon recoils against the photon, that the opening angle averages to $\pi/2$. The vector case behaves normally, and the gluons must be parallel as they recoil against the photon in the $x_1 \to 1$ limit where the photon has half the decay energy. The QCD $\langle \cos\theta_{23} \rangle$ behavior is, in fact, practically indistinguishable from the phase space prediction.

(e) Average thrust

$\Upsilon$ decay into hadrons produces events which are more planar than the background events [4]. There is an associated decrease in thrust on the $\Upsilon$ resonance compared to the thrust of $e^+e^- \to$ hadron events off the $\Upsilon$ resonance [4]. This evidence supports the QCD picture that the final state in $\Upsilon$ decay originates from 3 gluons. A well defined event plane is necessary for extracting azimuthal and polarization dependence in quarkonium decay into $\gamma$ + hadrons, and we plot the average thrust in Fig. 10 as a function of $x_1$ to indicate the degree of expected planarity. Average thrust is defined as

$$\langle T(x_1) \rangle = \frac{\int T\sigma(x_2)dx_2}{\int \sigma dx_2}$$

where $T = x_1$, $x_2$ or $x_3$, depending on which is largest. The integration limits of the numerator depend upon whether $x_1$ is the largest, intermediate, or smallest energy. For each $x_1$ value, the integration region has two parts corresponding to the possibilities $x_2 > x_3$ or $x_3 > x_2$. The QCD prediction is seen to lie below the scalar model prediction at every $x_1$-value - another demonstration of the two-jet-like aspect of the scalar case. The QCD curve, incidentally, is almost identical to phase space, as was the case in $\langle \cos\theta_{23} \rangle$ discussed above.

The average of $\langle T \rangle$ over various $x_1$ regions - "grand average" thrust $\ll T \gg$ - is shown as a function of $x_1^c$ in Fig. 8a. For example, if the data is averaged over the photon energy inverval $0.5 \leq x_1 \leq 1$, QCD predicts that $\ll T \gg = 0.82$, where

$$\ll T \gg \equiv \frac{\int_{x_1^c}^{1} \langle T \rangle \sigma \, dx_1}{\int_{x_1^c}^{1} \sigma \, dx_1}$$

The corresponding plot in the scalar gluon case is shown in Fig. 8b.

(f) Polarization asymmetry

So far we have only discussed measurements where the photon polarization is not detected. In order to extract the photon-polarization dependent observables $\sigma_{\parallel}(x_1)$ and $\sigma_{\perp}(x_1)$, a polarization sensitive measurement must be made, and the asymmetry $A = (\sigma_{\parallel} - \sigma_{\perp}) / (\sigma_{\parallel} + \sigma_{\perp})$ is the most accessible to direct measurement. To measure A, one must measure the difference between the number of events with linear photon polarization in the event plane and the number



of events with linear photon polarization perpendicular to the event plane.

In Fig. 11a we show the variation of the asymmetry parameter over the Dalitz plot in the case of the QCD prediction, and in Fig. 11b we show the corresponding plot in the case of the scalar gluon model prediction. The asymmetry is largest in the large $x_1$ region of the Dalitz plot in the QCD prediction. The scalar prediction is largest in the small $x_1$ region, giving a distribution which is easily distinguishable from that of QCD. For orientation we note that the maximum asymmetry in the QCD case occurs for values $x_1 = x_2 = x_3 = 2/3$, where $A = -0.5$, while the maximum occurs in the scalar case for values $x_1 = 0$, $x_2 = x_3 = 1$ where $A = -0.6$. We note that the QCD asymmetry distribution plotted in Fig. 11a is in agreement with that of Brodsky, DeGrand and Schwitters, Ref. 3.

The quantities $\sigma_{\parallel} - \sigma_{\perp}$, Table II, are integrated over the gluon energies and presented as functions of $x_1$ in Table IV for the QCD case and in the Appendix for the scalar gluon case.

We plot next the asymmetry as a function of $x_1$ in Fig. 12, and the QCD and scalar gluon results are seen to be distinctively different. The remarkable fact is that the asymmetry is large and negative, 30 % - 40 %, over just the range $0.5 < x_1 < 0.9$ of photon energies which is acceptable (in both the general and technical senses) experimentally. In both cases the photon is polarized perpendicular to the event plane.

Comparing Figs. 11 and 12, one notes further that, since Fig. 12 represents an average over all gluon energies, there are regions of the Dalitz plot

where the asymmetry is larger than 40 %. One can tune the asymmetry optimally if events near the center of the Dalitz plot are selected. Whatever data sample one uses, the observation of a negative asymmetry in the $0.5 < x_1 < 1$ region would be strong support for the picture of quarkonium decay via the QCD mechanism shown in Fig. 1.

So far we have restricted ourselves to consideration of the total asymmetry, which is obtained by integrating over all angles (refer to Eq. 4). Angular dependence of the asymmetries is determined by $\sigma_u^-$, $\sigma_L^-$, $\sigma_T^-$ and $\sigma_I^-$, and we display these cross-sections as functions of $x_1$ in Fig. 13a and Fig. 13b for the QCD and scalar cases, respectively. In the scalar gluon model, $\sigma_T^-$ is related to $\sigma_u^+$ by

$$\sigma_u^+ = -\frac{1}{2}\sigma_T^- \qquad (11)$$

and it is clear that $\sigma_T^-$ is the dominant asymmetry cross-section as $x_1 \to 1$. In the QCD case, $H_{++-;+}$ and $H_{+-+;+}$, Eq. 3a, are dominant as $x_1 \to 1$. All others have factors of $(1-x_1)$ and go to zero as $x_1 \to 1$. One sees that (11) holds in this $x_1 \to 1$ limit for QCD, and since $\sigma_u^+$ is large as $x_1 \to 1$ (Fig. 6a) then $\sigma_T^-$ is also large and negative in this limit. The implications of the large $\sigma_T^-$ values for the angular dependence of the asymmetry is discussed below.

Considering first the $\theta$-dependence of the asymmetry, obtained by integrating over the azimuthal angle $\chi$ (see Eq. 4 and Fig. 2), we show the asymmetry as a function of $\cos\theta$ for several different values of the scaled photon energy, $x_1$, in Fig. 14. One sees that in the vector gluon case, where the asymmetry effect is predicted to be large for large $x_1$ values, the $\theta = \pi/2$ configuration is optimal, but not significantly larger than the average asymmetry from the



experimental standpoint. In other words, the $\cos\theta$ plot shows that little sensitivity to the polarization resulting from dynamics is lost in the integration over $\theta$ angles. However, referring to Fig. 13 and Eq. 4, it is clear that the large $\sigma_T^-$ values near $x_1 = 1$ will produce strong azimuthal correlations which get lost in the polar angle distribution, in which the $\chi$-dependence is integrated out.

In order to extract the dependence on azimuth, we take an indirect route and use the relations (10) which relate the $\theta$ and $\hat{\theta}$ correlation cross-sections [2]. Taking the normal to the event plane as the z-axis we have then

$$A(\cos\hat{\theta}, x_1) = \frac{\hat{\sigma}_u^- (1+\cos^2\hat{\theta}) + 2\hat{\sigma}_L^- (1-\cos^2\hat{\theta})}{\hat{\sigma}_u^+ (1+\cos^2\hat{\theta}) + 2\hat{\sigma}_L^+ (1-\cos^2\hat{\theta})}$$

and, using (10), obtain

$$A(\cos\hat{\theta}, x_1) = \frac{(\frac{3}{2}\sigma_u^- + \sigma_L^- + \sigma_T^-) + \cos^2\hat{\theta}(-\frac{1}{2}\sigma_u^- + \sigma_L^- - 3\sigma_T^-)}{(\frac{3}{2}\sigma_u^+ + \sigma_L^+ + \sigma_T^+) + \cos^2\hat{\theta}(-\frac{1}{2}\sigma_u^+ + \sigma_L^+ - 3\sigma_T^+)} \qquad (12)$$

The result is plotted vs. $\cos^2\hat{\theta}$ for several $x_1$ values in Fig. 15. We note that limiting cases (i) $\cos^2\hat{\theta} = 0$, $x_1 \to 1$ where $A \to -1/3$ for both scalar and QCD predictions since $\sigma_T^- = -\frac{1}{2}\sigma_u^+$ in this limit (Eq. 11), and (ii) $\cos^2\hat{\theta} = 1$, $x_1 \to 1$ where $A = -2\sigma_T^-/\sigma_u^+ \to 1$ ! The QCD $\cos^2\hat{\theta}$ distribution changes rapidly as $x_1 \to 1$ and is practically the same at $x_1 = 1$ as the $x_1 = 0.9$ curve of the scalar case in Fig. 15.

The polarization asymmetries are strong, even in average quantities, and

afford a rich source of detailed information about the dynamics of quarkonium decay.

The photon polarization asymmetry is difficult to measure, so we wish to comment on two classic techniques that use the relationship between the photon polarization plane and the orientation of the $e^+e^-$ pair produced by a polarized photon either by conversion on a nuclear Coulomb field or "internally" (virtual photon). We first take up some features of the Bethe-Heitler conversion on a nucleus under heading (i) below and then remark under heading (ii) on the Dalitz or "internal" conversion process.

(i) Yang [20] and Berlin and Mandansky [21] pointed out thirty years ago that the correlation between the plane of production of an $e^+e^-$ pair and the polarization plane of the photon by which they are produced can determine the polarization of high energy photons. Wick [22] subsequently discussed the problem in the Weizsäcker-Williams approximation and estimated that the ratio R of the number of approximately coplanar pairs which lie in the plane of photon polarization to the number of approximately coplanar pairs which are perpendicular to the polarization plane is 4/3. Subsequent detailed studies [23] indicated that this was an over-estimate. The screened nucleus results appropriate to very small momentum-transfer squared, $q^2$, lower R to typically 1.2, though larger values can be obtained in special circumstances.

The Weizsäcker-Williams approximation effectively averages over a small range of the relative azimuthal angle between $e^+$ and $e^-$ (measured relative to the photon polarization plane) which is near $\pi$(coplanar $e^+e^-$) [22,23]. This averaging corresponds to an experimental sample of nearly coplanar $e^+e^-$ events. It was



stressed by Maximon and Olson [23] that this averaging must be done, because the high energy cross-section varies rapidly as a function of the (small) momentum transferred to the nucleus and therefore also as a function of the (small) acoplanarity angle.

To estimate the effect of the correlation ratio on an experimental determination of our theoretical polarization asymmetry $A = \frac{\sigma_{\parallel} - \sigma_{\perp}}{\sigma_{\parallel} + \sigma_{\perp}}$, we note that the $e^+e^-$ plane correctly identifies the photon polarization plane with probability $\frac{R}{1+R}$ ($R > 1$ is the "in plane/out of plane" ratio). The observed A would then be $\sigma_{\perp} \cdot \left(\frac{R}{1+R}\right) + \sigma_{\parallel} \cdot \frac{1}{R}$, for example. We then find

$$A_{observed} = \frac{R-1}{R+1} \cdot \left(\frac{\sigma_{\parallel} - \sigma_{\perp}}{\sigma_{\parallel} + \sigma_{\perp}}\right)_{Theoretical}$$

$$\approx \frac{1}{7} \cdot \left(\frac{\sigma_{\perp} - \sigma_{\parallel}}{\sigma_{\perp} + \sigma_{\parallel}}\right)_{Theoretical}$$

when one uses R = 4/3 as estimated by Wick.

(ii)
In charmonium decays into $e^+e^-$ + two gluons, where the $e^+e^-$ result from a virtual photon, a similar factor must be included to make the connection between the theoretical polarization asymmetry and the observed one. The effect can be readily found by considering $\gamma^* \longrightarrow e^+e^-$ in the rest frame of the $e^+e^-$ pair and noting that a boost along $\vec{p}^*_{\gamma}$ does not affect the correlation.

With a photon polarized along the x-axis and the $e^+e^-$ direction having azimuth $\phi$ with respect to x, one finds

$$\frac{d\Gamma}{d\phi} \sim \left(\frac{2}{3}\cos^2\phi - 1 - \frac{8m^2}{3q^2}\cos^2\phi\right)$$

$$\rightarrow \left(\frac{2}{3}\cos^2\phi - 1\right) \quad \text{when } q^2 >> m^2.$$

The correlation coefficient is therefore R = 1/3 and

$$A_{observed} = -\frac{1}{2}\left(\frac{\sigma_{\parallel} - \sigma_{\perp}}{\sigma_{\parallel} + \sigma_{\perp}}\right)_{Theoretical}.$$

The stronger correlation between the produced $e^+e^-$ -plane and the photon polarization plane in the direct conversion makes up some of the $O(\alpha)$ loss in event rate compared to the Bethe-Heitler conversion.

Clearly the study of possibilities to measure photon polarization is an involved one, requiring, for example, analysis of $q^2$ dependence of pair conversion vs. direct virtual photon decay in order to determine average opening angles at a given energy [24,25]. Such a detailed consideration is not our purpose here, where we simply wish to outline the problems associated with photon polarization determinations required by our proposed QCD tests. The experimental feasibility of determining the $e^+e^-$ plane will depend on details of the experimental set-up-granularity and dimensions of the detector and so forth, which we do not try to anticipate.

## IV. Conclusions

The decay of quarkonium $J^P = 1^{--}$ offers a rich source of information on the dynamics of quark-gluon interactions, and we have extended the calculation of



the $Q\bar{Q}(1^{--}) \rightarrow gg\gamma$ in both vector and scalar gluon models to include all of the decay structure function asymmetries. We found that the helicity formalism outlined in Sec. II simplifies such calculations greatly in comparison with the usual, basis-independent projection and tracing techniques.

The QCD predictions for the beam-event angular cross-sections showed that the beam-event angular correlation coefficients are comparable in magnitude and should be measurable in upcoming experiments. We placed strong emphasis on the polarization asymmetry calculation and its possible experimental measurement. The asymmetry was determined to be large over much of the Dalitz plot, Fig. 11a, and the asymmetry, which is negative, is plotted as a function of the photon energy $x_1$ and shows a maximum effect of $\approx$ 40 % in the experimentally accessible range, as seen in Figs. 12 and 14. The latter figure shows the asymmetry plotted vs. $\cos\theta$ for several different values of $x_1$. Because $\sigma_T^- \rightarrow -\frac{1}{2}\sigma_u^+$ as $x_1 \rightarrow 1$, and $\sigma_u$ is large, one predicts especially large polarization asymmetry near $\chi = \frac{\pi}{2}$ (see Eq. 4). This $\chi$-dependent effect is contained in $\hat{\theta}$ distributions, and we show this in Fig. 15 where $A \rightarrow 1$ as $\cos\hat{\theta}$ , $x_1 \rightarrow 1$.

These effects and the comparison, Figs. 6a, of the various correlation cross-sections lead us to conclude that detailed tests of QCD in quarkonium photon + hadrons are possible experimentally. For low mass states, the clean perturbative picture which we have used will be complicated by final state interactions among hadrons, of course, Resonant states [9] and/or gluon-gluon interactions will modify the QCD predictions.

Regarding scalar gluons, we found that the singular soft gluon region dominates the final state so much that the events are primarily composed of a hard photon

recoiling against one hard gluon. The transverse unpolarized cross-section $\sigma_u$, which has the singularity, dominates the other cross-sections so much that the angular correlation and asymmetry effects are washed out. Figs. 4, 6b, 11b and 12 illustrate this result. The average thrust, shown in Fig. 10, is clearly and measurably higher in the scalar than in the QCD case.

Finally, we remark that effects, expected to arise at high energy due to $Z^0 \leftrightarrow \gamma$ interference effects, and which should be taken into account in discussing $t\bar{t}$ decay, leave the polar ($\cos^2\theta$) distributions of the photon and its linear polarization unaffected. More complex density matrices resulting from beam polarization and/or inclusion of weak effects have been analysed by Körner and Schiller [26].

Acknowledgement

We would like to thank K.Koller, M.Krammer, G.Weber, G.Wolf and Y.Zaitsev for some useful discussions.



Appendix A: The Scalar Gluon Case

The matrix element $M_{ij}$ for $Q\bar{Q}(1^{--}) \to \gamma$ + two scalar gluons can be easily calculated from the Feynman diagram of Fig. 1. It results in the same covariant trace as in Eq. (1) with $\alpha_s$ replaced by the effective scalar coupling constant $\bar{\alpha}_s$ and the omission of the polarization vector terms $\not{\epsilon}_2^*$ and $\not{\epsilon}_3^*$. The effective fermion-scalar gluon coupling is defined by $\bar{\alpha}_s \bar{\psi} \frac{\lambda^i}{2} \psi s^i$. The trace calculation yields

$$M_{ij} = -8 N_{ij} \frac{1}{x_1 x_2 x_3} \left\{ (1-x_3 x_3) e \cdot e_i^* + \frac{1}{2m^2} \left[ (1-x_3)(p_1 \cdot e)(p_2 \cdot e_i^*) + x_1 (p_2 \cdot e)(p_2 \cdot e_i^*) \right] \right\} \quad \text{(A.1)}$$

where $N_{ij}$ is a normalization factor defined after Eq. (1). The helicity amplitudes $H_{\lambda_\gamma; \lambda_{Q\bar{Q}}}$ are given by

$$\begin{aligned} H_{+;+} &= -8 N_{ij} \cdot \frac{1}{x_1^2 x_2 x_3} \cdot \left[ x_1 (1 - x_2 x_3) - X \right], \\ H_{-;+} &= -8 N_{ij} \cdot \frac{1}{x_1^2 x_2 x_3} \cdot X \end{aligned} \quad \text{(A.2)}$$

and

$$H_{+;0} = 4\sqrt{2}\, N_{ij} \cdot \frac{1}{x_1^2 x_2 x_3} \cdot X^{1/2} \cdot (x_2 - x_3)$$

where $X \equiv (1-x_1)(1-x_2)(1-x_3)$. The parity conditions are

$$\begin{aligned} H_{-\lambda_\gamma;-} &= H_{+\lambda_\gamma;+} \\ H_{-\lambda_\gamma;0} &= -H_{\lambda_\gamma;0} \end{aligned} \quad \text{(A.3)}$$

In Table (A.1) we list the expressions for the unpolarized photon cross-sections which appear in Eq. (4). Since there are only three independent helicity amplitudes and these are real in Born approximation, (A.2), there are clearly many relationships among the eight $\sigma_i^{\pm}$. We write, therefore, all of the $\sigma_i^-$ in terms of $\sigma_i^+$ quantities in Table A.II.

Because the photon spectrum is more readily measurable than the double Dalitz distributions, we show the expressions for cross-sections which result after integration over gluon variables in Table A.III in the unpolarized photon case. The integrated $\sigma_i^-$ are related to the $\sigma_i^+$ in the same way as shown in Table A.II.

As remarked in the text and as is evident in Figs. 3b and 4, the scalar gluon rate blows up at $x_1 \to 1$ as $1/(x_1-1)$. To compute the total rate, we cut off the $x_1$ integration according to $\Delta \le x_1 \le 1-\Delta$, the lower cutoff included for uniformity in comparing with the three gluon case, where one needs the lower cutoff. The cutoff dependent expression for the total rate as a function of cutoff, referred to as $I^{gg\gamma}(\Delta)$ in the text, is defined by (see also Eq.4)

$$\begin{aligned}\Gamma_{ij}^{gg\gamma} &= \frac{m}{6\pi^3}N_{ij}^2\Big\{\frac{1}{8}\big[\mathcal{L}_2(1-\Delta)-\mathcal{L}_2(-1+\Delta)+\mathcal{L}_2(-\Delta)-\mathcal{L}_2(\Delta)+\ln(1-\Delta)\ln(2-\Delta)\big]\\ &+\ln\Delta\ln(1+\Delta)+\ln\Delta\Big[-2+\frac{3}{4}\frac{\Delta}{1+\Delta}+\frac{5}{4}\cdot\frac{\Delta}{(1+\Delta)^2}-\frac{9}{4}\frac{\Delta}{1-\Delta}\Big]\\ &+\ln(1-\Delta)\Big[2-\frac{3}{4}\frac{(1-\Delta)}{2-\Delta}-\frac{5}{4}\frac{(1-\Delta)}{(2-\Delta)^2}+\frac{9}{4}\frac{(1-\Delta)}{\Delta}\Big]\\ &-\frac{5}{4}\cdot\frac{1}{1+\Delta}+\frac{5}{4}\cdot\frac{1}{2-\Delta}\Big\}\\ &\equiv \frac{m}{6\pi^3}N_{ij}^2 I^{gg\gamma}(\Delta)\end{aligned} \tag{A.4}$$

where $\Delta$ is the photon energy cutoff and $\mathcal{L}_2(x) = -\int_0^x \frac{\ln(1-x')dx'}{x'}$ is the dilogarithm function.



Since we are interested also in the branching ratio of the $\gamma$-inclusive decay involving scalar gluons, we briefly recapitulate the total rate calculation $Q\bar{Q}(1^{--}) \to$ three scalar gluons [16]. On evaluation of the Feynman diagram Fig. 1 corresponding to the three gluon case, one has

$$M_{ijk} = N_{ijk}\,Tr\big\{2m[\not\epsilon(\not p-m)(-\not p+\not p_3-m)^{-1}(\not p-\not p_1-m)^{-1}]+\text{cycl. perm}\big\}$$

$$= N_{ijk}\frac{4}{m}\cdot\frac{1}{x_1x_2x_3}\cdot\big(-p_1\cdot\epsilon(x_2-x_3)+p_2\cdot\epsilon(x_1-x_3)-p_3\cdot\epsilon(x_1-x_2)\big)$$

where $N_{ijk} = \frac{1}{2}f_{ijk}\cdot 2\sqrt{2}(\tilde{\alpha}_s 4\pi)^{3/2}\psi(0)/(m^{3/2}\Gamma_3)$. The helicity amplitudes are

$$H_+ = 4\sqrt{2}\,N_{ijk}\frac{\sqrt{X}}{x_1^2x_2x_3}(3x_1-2)$$

$$H_0 = 8\,N_{ijk}\cdot\frac{1}{x_1^2x_2x_3}\cdot(x_2-x_3)(2x_1-1)$$

and the parity condition is $H_- = -H_+$. We shall only give the result for $\sigma^- = \sigma_u^- + \sigma_L^-$ for the total rate calculation, Eq. 4-

$$\sigma = 64N_{ijk}^2\cdot\frac{1}{x_1^2x_2^2x_3^2}\big[x_2x_3(5-9x_1)-(4-10x_1+5x_1^2)\big]$$

where $N_{ijk}^2 = \frac{N^2}{4}f_{ijk}f_{ijk} = 6N^2$. Integration over $x_2$ and $x_1$ then yields the expression for the total rate, including a statistics factor 1/6,

$$\begin{aligned}\Gamma^{ggg}(\Delta) &= \frac{m}{24\pi^3}N_{ijk}^2\Big\{3\big[-\mathcal{L}_2(1-\Delta)+\mathcal{L}_2(-1+\Delta)+\mathcal{L}_2(\Delta)-\mathcal{L}_2(-\Delta)+\ln(1-\Delta)\ln(2-\Delta)\big]\\ &-\ln\Delta\ln(1+\Delta)+\frac{4}{3}\ln(1-\Delta)\Big[1-\frac{3}{2}\frac{1}{\Delta}+\frac{3}{2-\Delta}-\frac{1}{(2-\Delta)^2}\Big]\\ &+\frac{4}{3}\ln(\Delta)\Big[-1+\frac{3}{2}\frac{1}{1-\Delta}-\frac{3}{1+\Delta}+\frac{1}{(1+\Delta)^2}\Big]+\frac{4}{3}\Big(\frac{1}{1+\Delta}-\frac{1}{2-\Delta}\Big)\Big\}\\ &\equiv \frac{m}{24\pi^3}N_{ijk}^2 I^{ggg}(\Delta)\end{aligned} \tag{A.5}$$

## Appendix B: Linear Photon Polarization in the x=y Plane

In general the (unnormalized) photon density matrix $\rho_{\lambda\lambda'}$ will involve four independent components, viz.

$$\rho_{\lambda\lambda'} = \frac{1}{2}\left(\sigma \mathbb{1} + \rho_x \sigma_x + \rho_y \sigma_y + \rho_z \sigma_z\right) \tag{B1}$$

A circular polarization component $\rho_z$ will only be present when parity violating or longitudinal beam polarization effects are included[26]. The y-component corresponding to linear photon polarization in the x=y plane has not been considered in the main text since it does not contribute to the polar distributions worked out in this paper. For the sake of completeness we will list the relevant y-components in this Appendix.

The double differential density matrix distribution is given by[26]

$$\frac{d\rho}{dx_1 dx_2 d\cos\theta d\chi} \sim \frac{3}{8}(1+\cos^2\theta)(\sigma_u \mathbb{1} + \rho_{u_x}\sigma_x) + \frac{3}{4}\sin^2\theta(\sigma_t \mathbb{1} + \rho_{L_x}\sigma_x) \tag{B2}$$
$$+ \frac{3}{4}\sin^2\theta\cos 2\chi(\sigma_T \mathbb{1} + \rho_{Tx}\sigma_x) - \frac{3}{4}\sin^2\theta\sin 2\chi\,\rho_{4y}\sigma_y$$
$$+ \frac{3}{2\sqrt{2}}\sin 2\theta\sin\chi\,\rho_{5y}\sigma_y - \frac{3}{2\sqrt{2}}\sin 2\theta\cos\chi(\sigma_I \mathbb{1} + \rho_{Ix}\sigma_x).$$

One notes from Eq.(B2) that the $\rho_y$ contribution drops out after $\chi$-integration as stated above.

The y-components of the density matrix can be expressed in terms of the x-components given in Tables II and AII with $\sigma^{\parallel} - \sigma^{\perp} = -\rho_x$.

QCD:
$$\rho_{4y} = \rho_{Tx}\,[1-(1-x_1)^2]/[1+(1-x_1)^2]$$
$$\rho_{5y} = \rho_{Ix}\,x_1/(2-x_1)$$



Scalar Gluon:
$$\rho_{4y} = \rho_{Tx}\cdot(H_{+;+}^2 - H_{-;+}^2)/(H_{+;+}^2 + H_{-;+}^2)$$
$$\rho_{5y} = \rho_{Ix}\cdot(H_{+;+} + H_{-;+})/(H_{+;+} - H_{-;+})$$

The effect of the y-components can be judged by considering the general parametrization of the (normalized) density matrix of a linearly polarized photon:

$$\rho = \frac{1}{2}\left(\mathbb{1} + P_{lin}(\cos 2\varphi\,\sigma_x + \sin 2\varphi\,\sigma_y)\right) \tag{B3}$$

From Eq.(B3) one concludes that the polarization plane has an angle $\varphi = \frac{1}{2}\,\mathrm{arcctg}(\rho_x/\rho_y)$ relative to the decay plane and the degree of polarization in this plane is given by $P_{lin} = (\rho_x^2 + \rho_y^2)^{1/2}/\sigma$.

References


1. M. Chanowitz, Phys. Rev. D12 (1975) 912.

2. K. Koller and T. Walsh, Nuclear Phys. B140 (1978) 449.

3. S. Brodsky, D.G. Coyne, T.A. DeGrand and R.R. Horgan, Phys. Lett. 70B (1977) 234; S. Brodsky, T.A. DeGrand and R.F. Schwitters, Physics Letters 79B (1978) 225.

4. Ch. Berger et al., Phys. Lett. 82B (1979) 449.

5. JADE Collaboration, W. Bartel et al., Phys. Lett. 91B (1980) 142.
MARK-J Collaboration, D.P. Barber et al., Phys. Rev. Lett. 43 (1979) 830.
PLUTO Collaboration, Ch. Berger et al., Phys. Lett. 86B (1979) 418.
TASSO Collaboration, R. Brandelik et al., Phys. Lett. 86B (1979) 243.

6. TASSO Collaboration, "Evidence for a spin 1 gluon in Three Jet Events", DESY 80/80, August 1980.
PLUTO Collaboration, "A Study of Multijet Events in $e^+e^-$ Annihilation", DESY 80/93, Oct. 1980.

7. G.S. Abrams et al., Phys. Rev. Lett. 44 (1980) 114. Also see G.J. Feldman, Proceedings of the XV Rencontre de Moriond, March 15-21, 1980 and SLAC-PUB-2510 (1980).

8. M.T. Ronan et al., Phys. Rev. Lett. 44 (1980) 367.

9. R. Partridge et al., Phys. Rev. Lett. 45 (1980) 1150.

10. G. Kramer, G. Schierholz and J. Willrodt, Phys. Lett. 78B (1978) 249.

11. R. Delbourgo, A. Salam and J. Strathdee, Proc. Roy. Soc. A278 (1965) 146; B. Sakita and K. Wali, Phys. Rev. Lett. 14 (1965) 404. For a quark model formulation see T. Gudehus, DESY Report 68/11 (1968) unpublished; Phys. Rev. 184, 1788 (1969).





12. M. Krammer, Phys. Lett. 74B (1978) 361; F.A. Berends and G.J. Komen, Nucl. Phys. B119 (1977) 112.

13. A. Ore and J.L. Powell, Phys. Rev. 75 (1949) 1696.

14. LENA Collaboration, "Total Width and Leptonic Branching Ratio of the $\Upsilon(9.46)$", DESY 80/53, June 1980.

15. M. Krammer and H. Krasemann, Proceedings of the XVIII Int. Univ. für Kernphysik, Schladming, Austria 1979.

16. PLUTO Collaboration, Ref. 6.

17. TASSO Collaboration, Ref. 6.

18. K. Koller and H. Krasemann, Phys. Lett. 88B (1979) 119.

19. T. Walsh and P. Zerwas, Phys. Lett. 93B (1980) 53.

20. C.N. Yang, Phys. Rev. 77 (1950) 722.

21. T.H. Berlin and L. Mandansky, Phys. Rev. 78 (1950) 623.

22. G.C. Wick, Phys. Rev. 81 (1951) 467.

23. H. Olsen and L.C. Maximon, Phys. Rev. 114 (1959) 887; L.C. Maximon and H. Olsen, ibid. 126 (1962) 310.

24. M. Kobayashi and K. Kondo, Nucl. Instruments and Methods, 104 (1972) 101; K. Kondo et al., ibid. 114 (1974) 365.

25. H. Olsen, Phys. Rev. 131 (1963) 406; A.P. Potylitsyn, Journal of Nuclear Physics 3 (1978) 721.

26. J. Körner and D. Schiller, DESY 80/ (1980)

$$\sigma \equiv \sigma_u + \sigma_L = \frac{2N_{ij}^2}{x_1^2 x_2^2 x_3^2} \cdot \left[ x_1^2 (1-x_1)^2 + x_2^2 (1-x_2)^2 + x_3^2 (1-x_3)^2 \right]$$

$$\sigma_L \equiv \sigma_L^{\parallel} + \sigma_L^{\perp} = \frac{4N_{ij}^2}{x_1^4 x_2^2 x_3^2} \left[ (1-x_2)^2 + (1-x_3)^2 \right] \cdot X$$

$$\sigma_T \equiv \sigma_T^{\parallel} + \sigma_T^{\perp} = \frac{1}{2} \sigma_L$$

$$\sigma_I \equiv \sigma_I^{\parallel} + \sigma_I^{\perp} = \frac{N_{ij}^2 \sqrt{2X}}{x_1^4 x_2^2 x_3^2} \left\{ (1-x_2)(1-x_3)(x_2-x_3) + (1-x_1)\left[ (1-x_2)^3 - (1-x_3)^3 \right] \right\}$$

Table I: The double differential decay cross-sections when polarization of the photon is not detected - QCD predictions. The arguments $x_i$ of the $\sigma_i$ are suppressed for convenience. $X \equiv (1-x_1)(1-x_2)(1-x_3)$ and $N_{ij}^2 \equiv N^2 \delta_{ij}\delta_{ij} = 8N^2$.

$$\sigma^- \equiv \sigma^{\parallel} - \sigma^{\perp} = -\frac{4N_{ij}^2}{x_1^2 x_2^2 x_3^2} \cdot X$$

$$\sigma_L^- \equiv \sigma_L^{\parallel} - \sigma_L^{\perp} = -\frac{8N_{ij}^2}{x_1^2 x_2^2 x_3^2} \cdot X \cdot (1-x_2)(1-x_3)$$

$$\sigma_T^- \equiv \sigma_T^{\parallel} - \sigma_T^{\perp} = -\frac{2N_{ij}^2}{x_1^4 x_2^2 x_3^2} \cdot (1-x_2)^2 (1-x_3)^2 \left[ 1 + (1-x_1)^2 \right]$$

$$\sigma_I^- \equiv \sigma_I^{\parallel} - \sigma_I^{\perp} = \frac{\sqrt{2}\, N_{ij}^2}{x_1^4 x_2^2 x_3^2} X^{1/2} (1-x_2)(1-x_3)(x_2-x_3)(2-x_1)$$

Table II: Difference between double differential in- and out-of-plane polarized photon cross-sections in QCD case.



$$\sigma \equiv \sigma^{\parallel} + \sigma^{\perp} = \frac{2N_{ij}^2 (1-x_1)}{x_1 (2-x_1)^3} \left\{ \frac{(2-x_1)^4}{1-x_1} + x_1^2 (2-x_1) + 2\left[ (2-x_1)^3 - (1-x_1)x_1^2 \right] \frac{\ln(1-x_1)}{x_1} \right\}$$

$$\sigma_L \equiv \sigma_L^{\parallel} + \sigma_L^{\perp} = -\frac{2N_{ij}^2 (1-x_1)}{x_1 (2-x_1)^3} \left\{ (2-x_1)\left[ 2 + 6\frac{(1-x_1)}{x_1^2} \right] + \left[ 6(1-x_1) + x_1^2 + 12\frac{(1-x_1)^2}{x_1^2} \right] \frac{\ln(1-x_1)}{x_1} \right\}$$

$$= \sigma_L^- - \sigma^- \quad \text{(see table IV)}.$$

$$\sigma_T \equiv \sigma_T^{\parallel} + \sigma_T^{\perp} = \frac{1}{2} \sigma_L$$

$$\sigma_I \equiv \sigma_I^{\parallel} + \sigma_I^{\perp} = \frac{N_{ij}^2 \sqrt{2}\sqrt{1-x_1}}{(2-x_1) x_1^3} \left[ (2-x_1)^2 + \frac{2(1-x_1)}{2-x_1} (2 - x_1 + x_1^2) - \sqrt{1-x_1}\,(2-x_1)(6-3x_1+x_1^2) \frac{\arcsin\left(\frac{x_1}{2-x_1}\right)}{x_1} \right]$$

Table III: Single differential cross-sections where the photon polarization goes undetected - QCD case. The argument $x_1$ of the $\sigma_i$ is suppressed, where $x_1$ is the scaled photon energy.

$$\sigma^- \equiv \sigma^{\parallel} - \sigma^{\perp} = \frac{4N_{ij}^2 (1-x_1)}{x_1 (2-x_1)^3} \left\{ 2 - x_1 + (2-2x_1+x_1^2) \frac{\ln(1-x_1)}{x_1} \right\}$$

$$\sigma_L^- \equiv \sigma_L^{\parallel} - \sigma_L^{\perp} = -\frac{4N_{ij}^2 (1-x_1)}{x_1^3 (2-x_1)^3} \left\{ (2-x_1)(6-6x_1+x_1^2) + 4(1-x_1)(3-3x_1+x_1^2) \frac{\ln(1-x_1)}{x_1} \right\}$$

$$\sigma_T^- \equiv \sigma_T^{\parallel} - \sigma_T^{\perp} = \frac{\left[ 1 + (1-x_1)^2 \right]}{4(1-x_1)} \sigma_L^-$$

$$\sigma_I^- \equiv \sigma_I^{\parallel} - \sigma_I^{\perp} = \frac{\sqrt{2}(2-x_1)\sqrt{1-x_1}}{x_1^3} \left\{ \frac{2(1-x_1)}{(2-x_1)^2} + 1 - \frac{3(1-x_1)}{x_1\sqrt{1-x_1}} \arcsin\left(\frac{x_1}{2-x_1}\right) \right\} N_{ij}^2$$

Table IV: Differences between in- and out of-plane polarized photon single differential cross-sections in QCD case.

$$\sigma^{\parallel} + \sigma^{\perp} = 64\, N_{ij}^2 \frac{1}{x_1^2 x_2^2 x_3^2} \cdot \left[ 2(1-x_2x_3)^2 - 3X \right]$$

$$\sigma_L^{\parallel} + \sigma_L^{\perp} = 64\, N_{ij}^2 \cdot \frac{1}{x_1^4 x_2^2 x_3^2} \cdot (x_2 - x_3)^2 \cdot X$$

$$\sigma_T^{\parallel} + \sigma_T^{\perp} = 128\, N_{ij}^2 \cdot \frac{1}{x_1^4 x_2^2 x_3^2} \left[ 1 - x_2x_3 - x_1(1-x_1) \right] \cdot X$$

$$\sigma_I^{\parallel} + \sigma_I^{\perp} = -32\sqrt{2}\, N_{ij}^2 \frac{X^{1/2}}{x_1^4 x_2^2 x_3^2} \left[ x_1(1-x_2x_3) - 2X \right](x_2 - x_3)$$

Table AI: Unpolarized photon double differential cross-sections in the scalar gluon model. $X = (1-x_1)(1-x_2)(1-x_3)$. Refer to Eq. 4 for the interpretation of the $\sigma_i$. Note $\sigma = \sigma_u + \sigma_L$. The $\sigma_i$ arguments $x_1$, $x_2$ and $x_3$ are suppressed for notational reasons.

$$\sigma^{\parallel} - \sigma^{\perp} = \sigma_L^{\parallel} + \sigma_L^{\perp} - 2(\sigma_T^{\parallel} + \sigma_T^{\perp})$$

$$\sigma_L^{\parallel} - \sigma_L^{\perp} = \sigma_L^{\parallel} + \sigma_L^{\perp}$$

$$\sigma_T^{\parallel} - \sigma_T^{\perp} = -\tfrac{1}{2}(\sigma_u^{\parallel} + \sigma_I^{\perp})$$

$$\sigma_I^{\parallel} - \sigma_I^{\perp} = \sigma_I^{\parallel} + \sigma_I^{\perp}$$

Table AII: Differences between double differential in and out of-plane photon polarization cross-sections in the scalar gluon model.



$$\sigma^{\parallel} + \sigma^{\perp} = \frac{64\, N_{ij}^2}{x_1(2-x_1)^2(1-x_1)} \cdot \left\{ 2 + 3(1-x_1)^2 + (1-x_1)(2-x_1)^2 + \frac{(1-x_1)^2}{2-x_1}\left[ 6 + 2x_1 + 3(2-x_1)^2 \right] \frac{\ln(1-x_1)}{x_1} \right\}$$

$$\sigma_L^{\parallel} + \sigma_L^{\perp} = -\frac{64\, N_{ij}^2 (1-x_1)}{x_1^3(2-x_1)} \left\{ 3(2-x_1) + \left[ 6(1-x_1) + x_1^2 \right] \frac{\ln(1-x_1)}{x_1} \right\}$$

$$\sigma_T^{\parallel} + \sigma_T^{\perp} = \frac{-64 N_{ij}^2 (1-x_1)}{x_1^3} \left\{ 1 + \frac{2(1-x_1+x_1^2)}{(2-x_1)^2} + \frac{2}{(2-x_1)} \left[ 1 + (1-x_1)^2 - \frac{2(1-x_1+x_1)^2(1-x_1)}{(2-x_1)^2} \right] \frac{\ln(1-x_1)}{x_1} \right\}$$

$$\sigma_I^{\parallel} + \sigma_I^{\perp} = \frac{32\sqrt{2}\, N_{ij}^2 (1-x_1)^{1/2}(2-x_1)}{x_1^3} \left\{ 1 + \frac{2(2-3x_1+2x_1^2)}{(2-x_1)^3} - \frac{1}{(1-x_1)^{1/2}} \left[ \frac{2(1-x_1)}{} + \frac{(2-3x_1+2x_1^2)}{(2-x_1)} \right] \left[ \arcsin\left( \frac{x_1}{2-x_1} \right) \right] / x_1 \right\}$$

Table AIII: Single differential cross-sections as a function of photon energy $x_1$ for unpolarized photons in the scalar model. The $x_1$ argument of $\sigma_i$ is suppressed.

Figure Captions

Fig. 1. The basic Feynman graph for the process: quarkonium $\rightarrow g+g+\gamma$ considered in this paper. $p_1$ always represents the photon momentum.

Fig. 2. The event coordinate system which we use to define angular correlations. When energy ordering is required, the x-axis is taken to be in the half-plane of the more energetic gluon.

Fig. 3. Dalitz plot distribution for $gg\gamma$ final state (a) vector gluons (b) scalar gluons.

Fig. 4. The photon energy spectra in the QCD case (solid line) and scalar case (dashed line). Both curves are normalized to 1 in the interval $[0,0.9]$ for purposes of comparison.

Fig. 5. Thrust distribution. Normalization as in Fig. 4.

Fig. 6. Beam-event correlation cross-sections $\sigma_u$, $\sigma_l$, $\sigma_T$ and $\sigma_I$ as a function of photon energy.
(a) Vector gluons. $\sigma = \sigma_u + \sigma_l$ normalized to 1 in $[0,1]$
(b) Scalar gluons. $\sigma = \sigma_u + \sigma_l$ normalized to 1 in $[0,0.9]$

Fig. 7. The photon polar angle distribution coefficient, $\alpha$, as a function of photon energy in the QCD case (solid line) and scalar model (dashed line).

Fig. 8. $\langle a \rangle$, $\langle\langle \text{thrust} \rangle\rangle$ and $\langle A \rangle$ as functions of $x_1^c$ ; (a) vector case and (b) scalar case.



Fig. 9. $\langle \cos \theta_{23} \rangle$ vs. $x_1$.

Fig. 10. $\langle$ thrust $\rangle$ as function of $x_1$.

Fig. 11. Dalitz plot distribution of polarization asymmetry (a) vector gluons (b) scalar gluons.

Fig. 12. The $x_1$-dependence of the polarization asymmetry in the QCD (solid line) and scalar (dashed) cases.

Fig. 13. $\sigma_i^{\parallel} - \sigma_i^{\perp}$ as functions of $x_1$ (a) vector gluons, (b) scalar gluons. Normalization as in Fig. 6.

Fig. 14. The $\cos\theta$ dependence of the polarization asymmetry for various $x_1$ values.

Fig. 15. The $\cos\hat{\theta}$ dependence of the polarization asymmetry. $\hat{\theta}$ is the angle between the normal to the event plane and the $e^-$ beam direction.

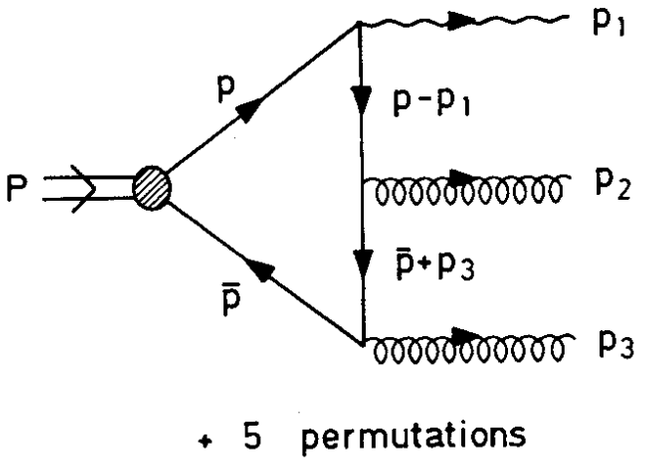


Fig.1

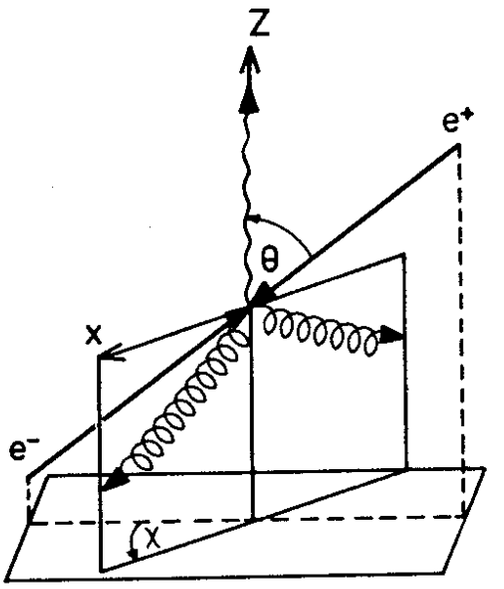


Fig. 2

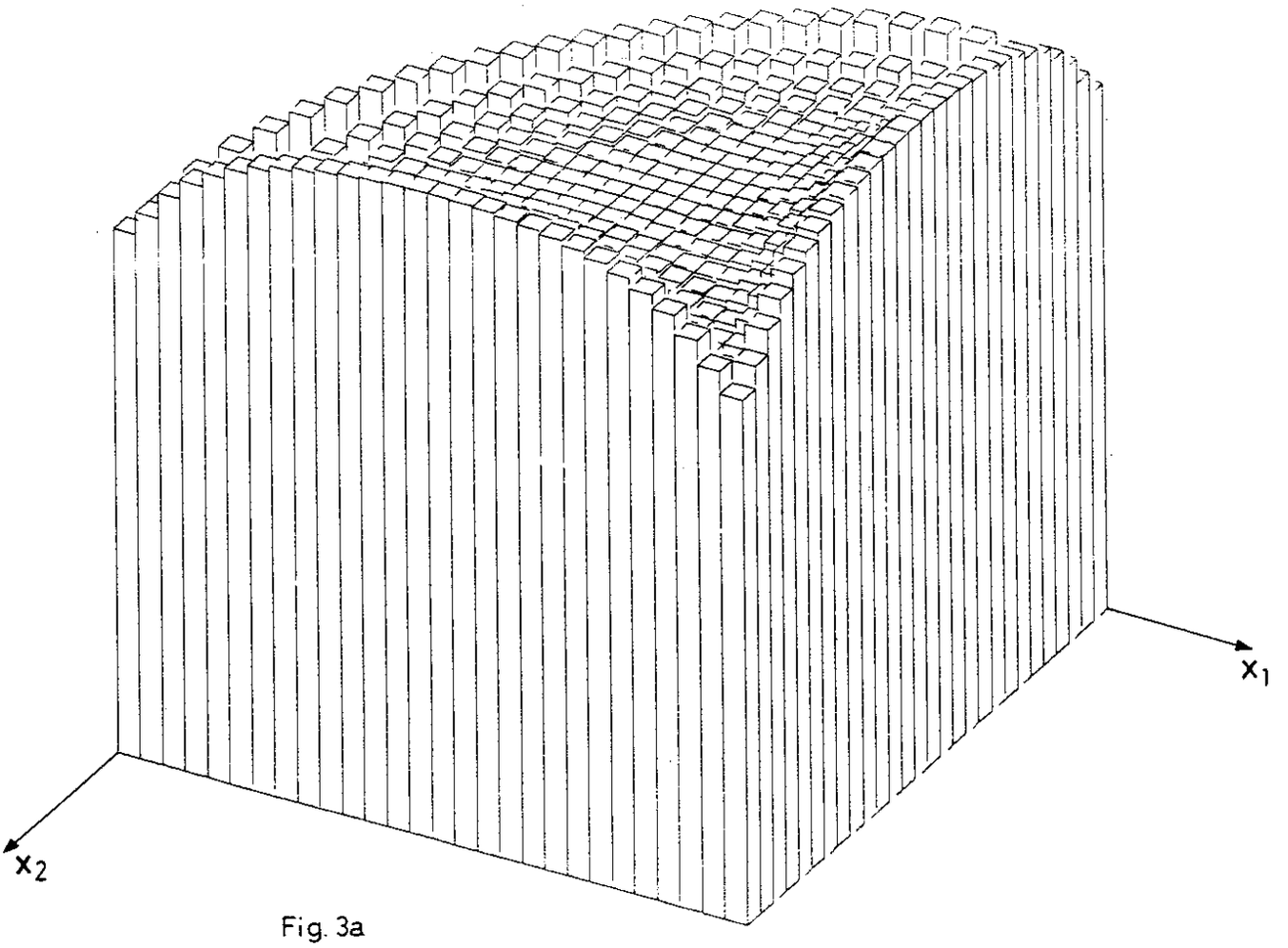


Fig. 3a

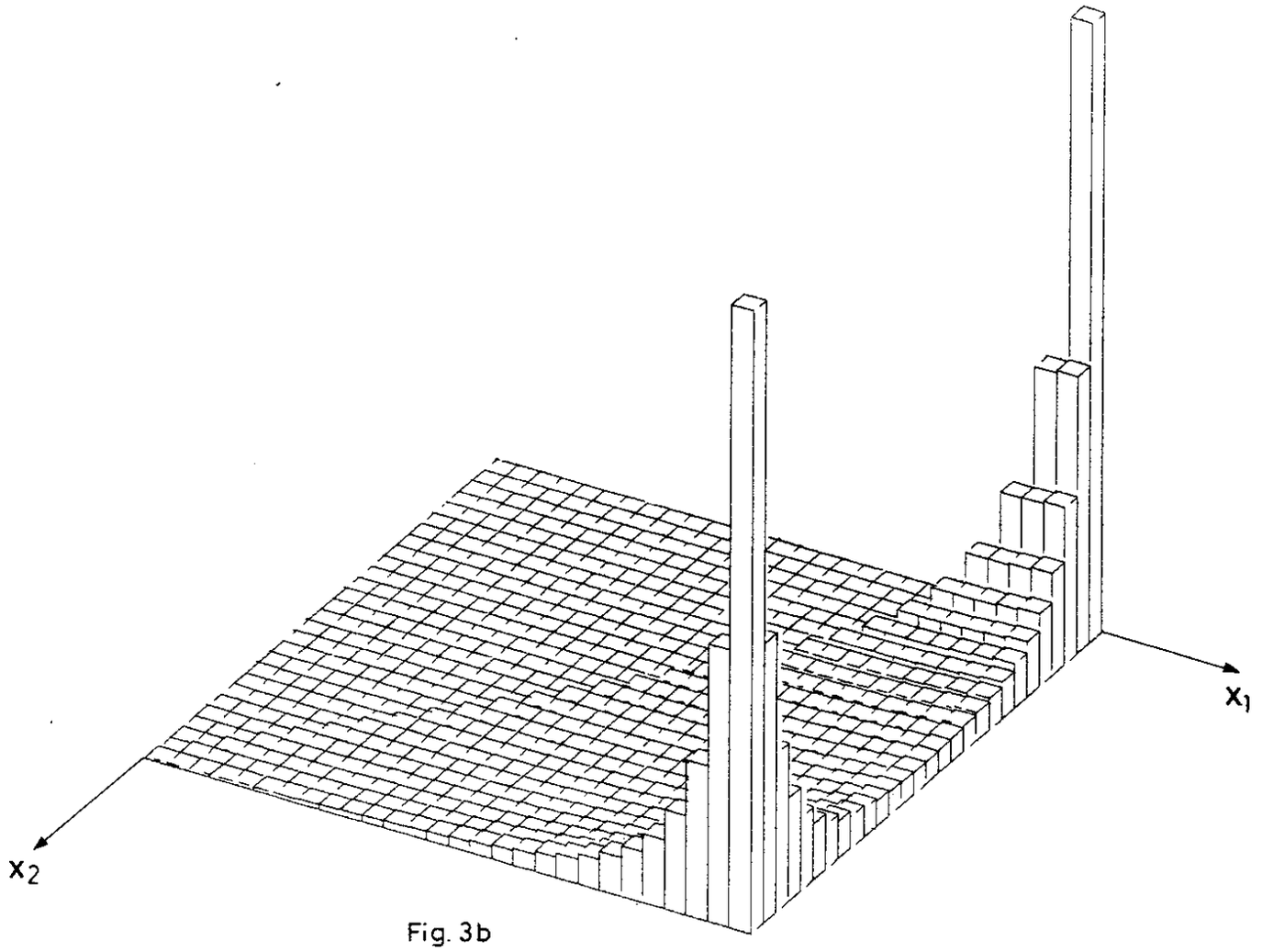


Fig. 3b

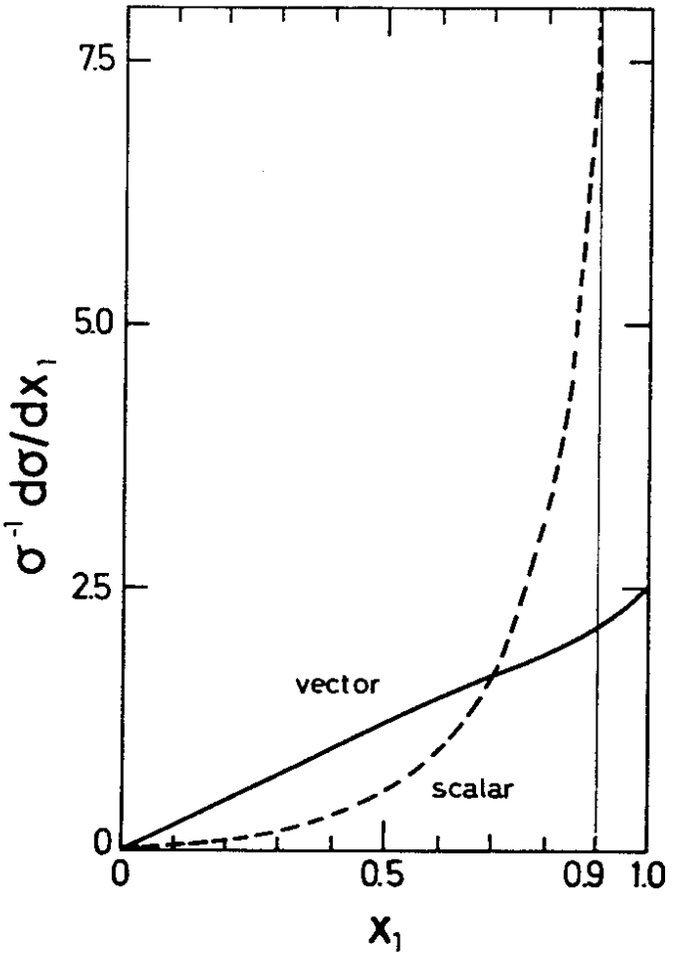


Fig. 4

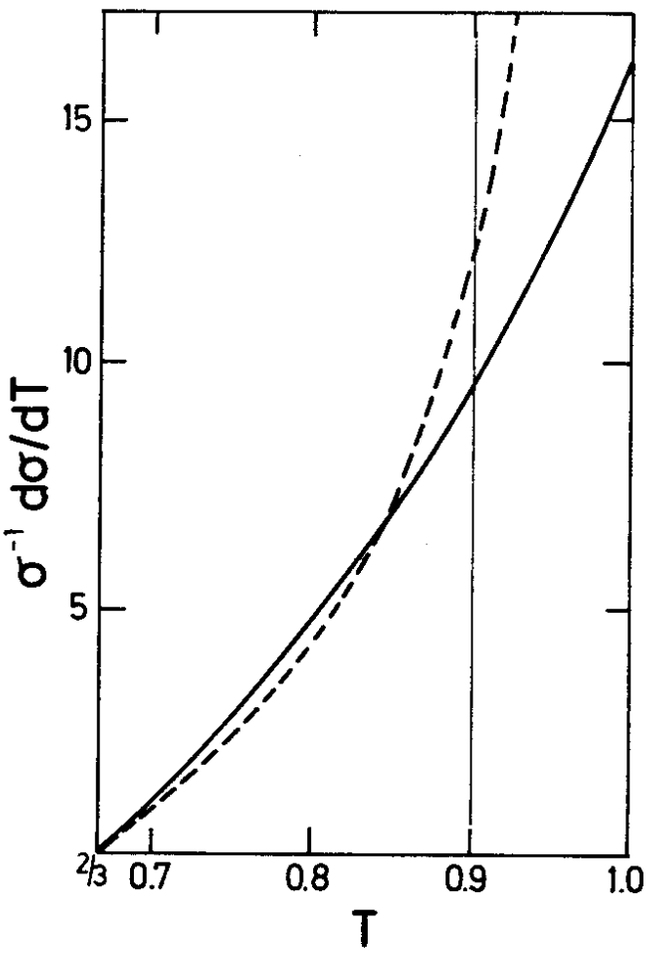


Fig. 5

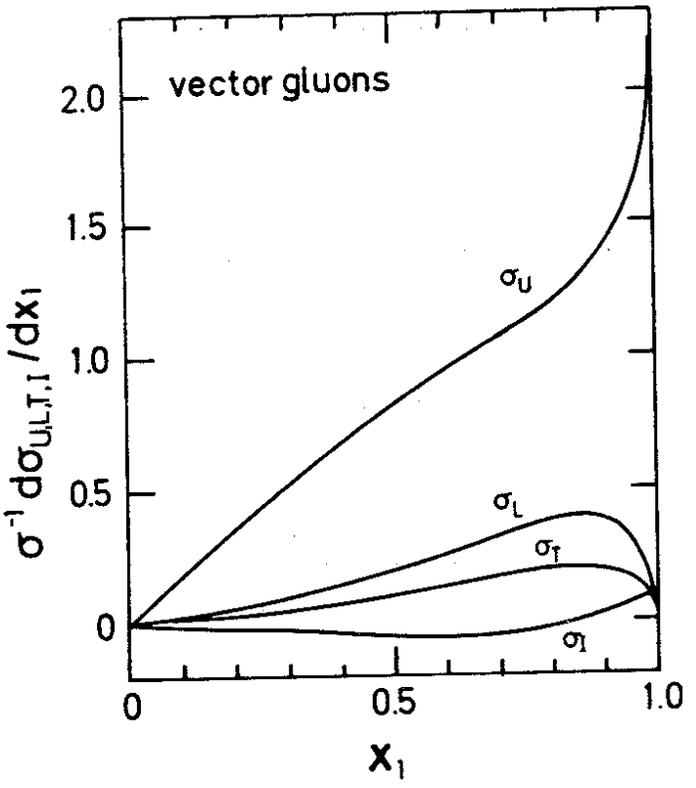


Fig. 6a

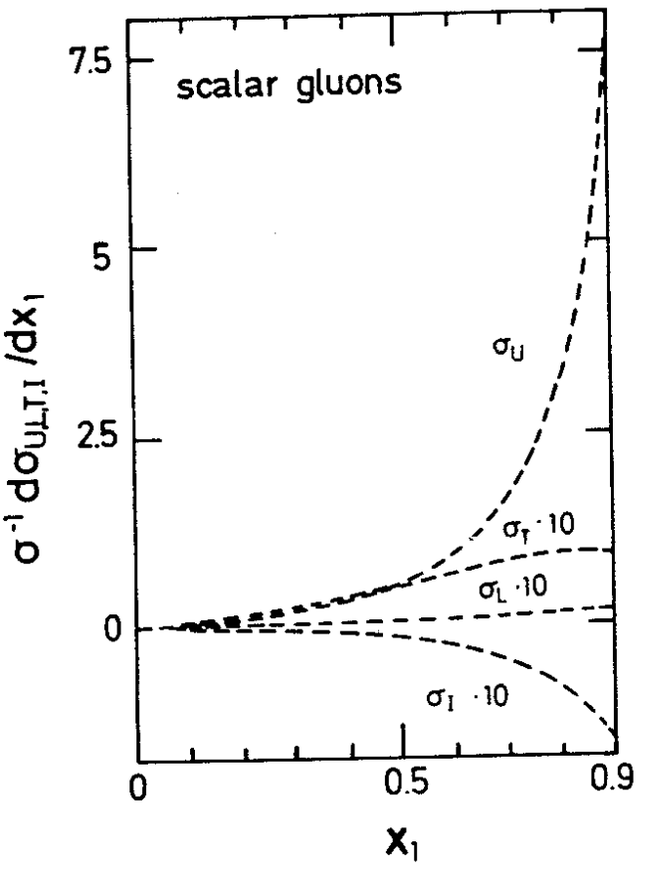


Fig. 6b

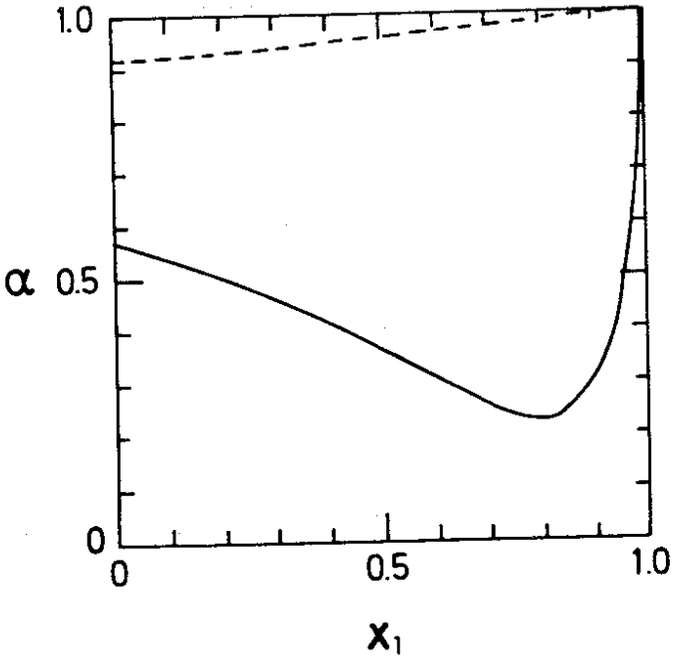


Fig. 7

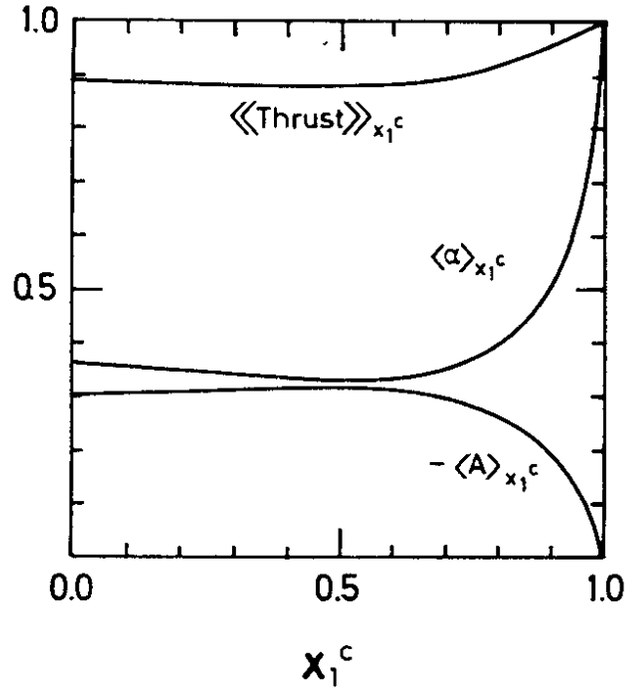


Fig. 8a

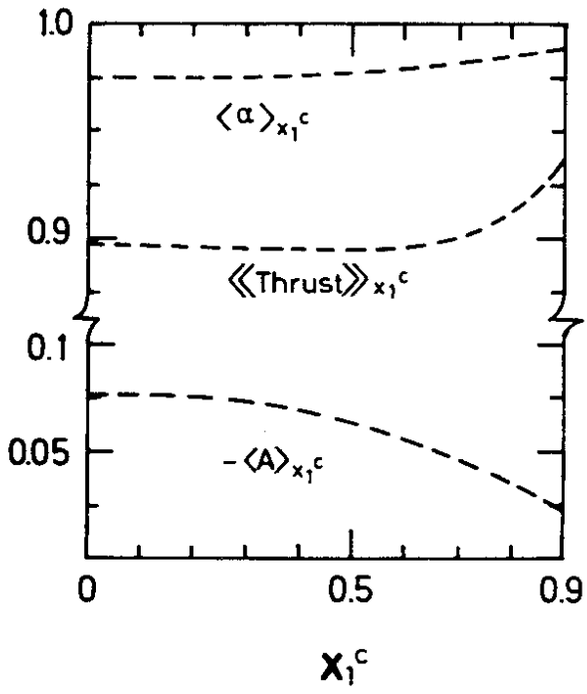


Fig. 8b

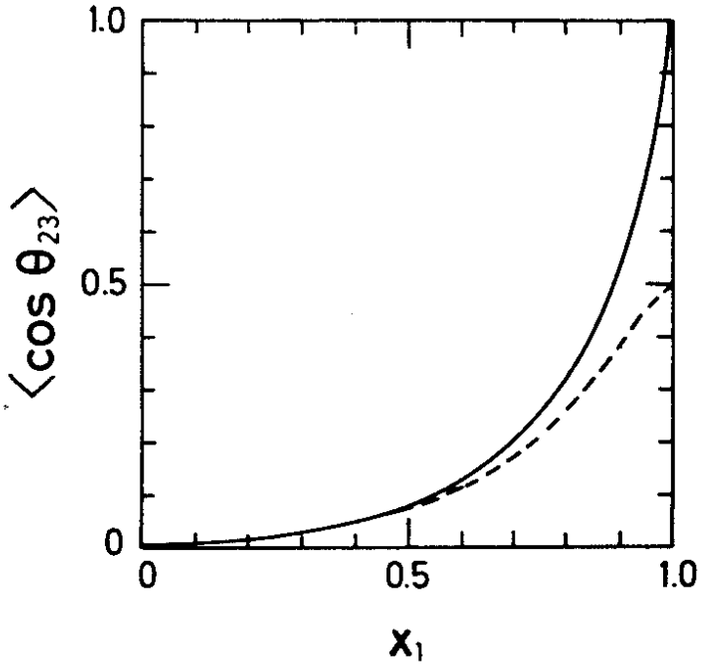


Fig. 9

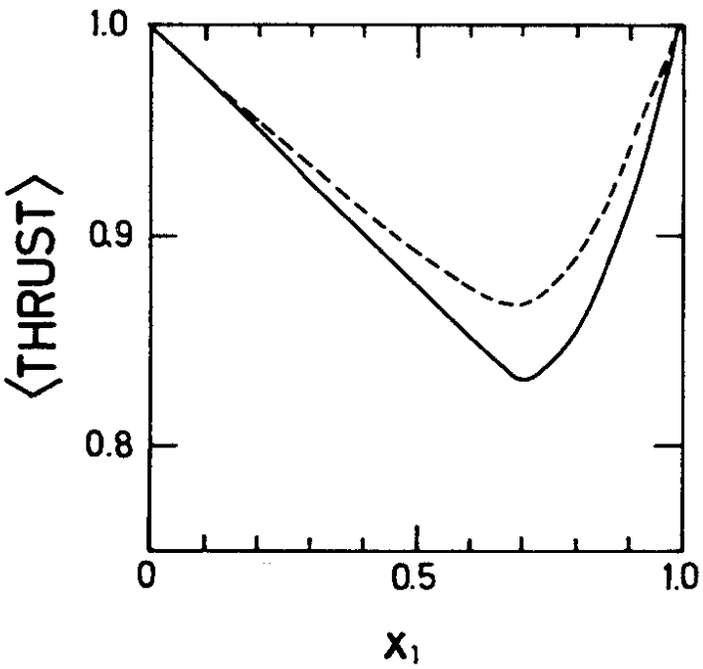


Fig. 10

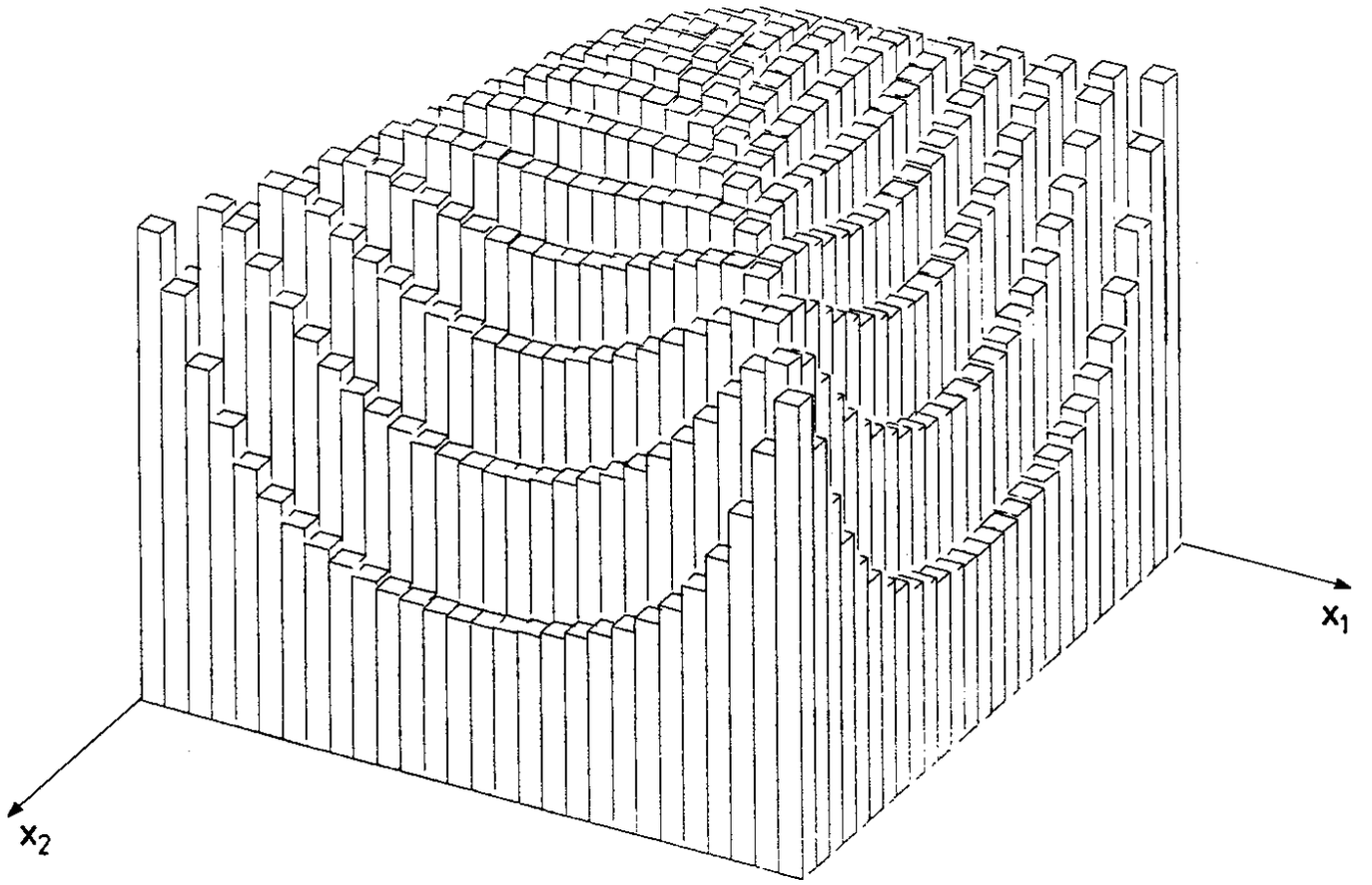


Fig.11a

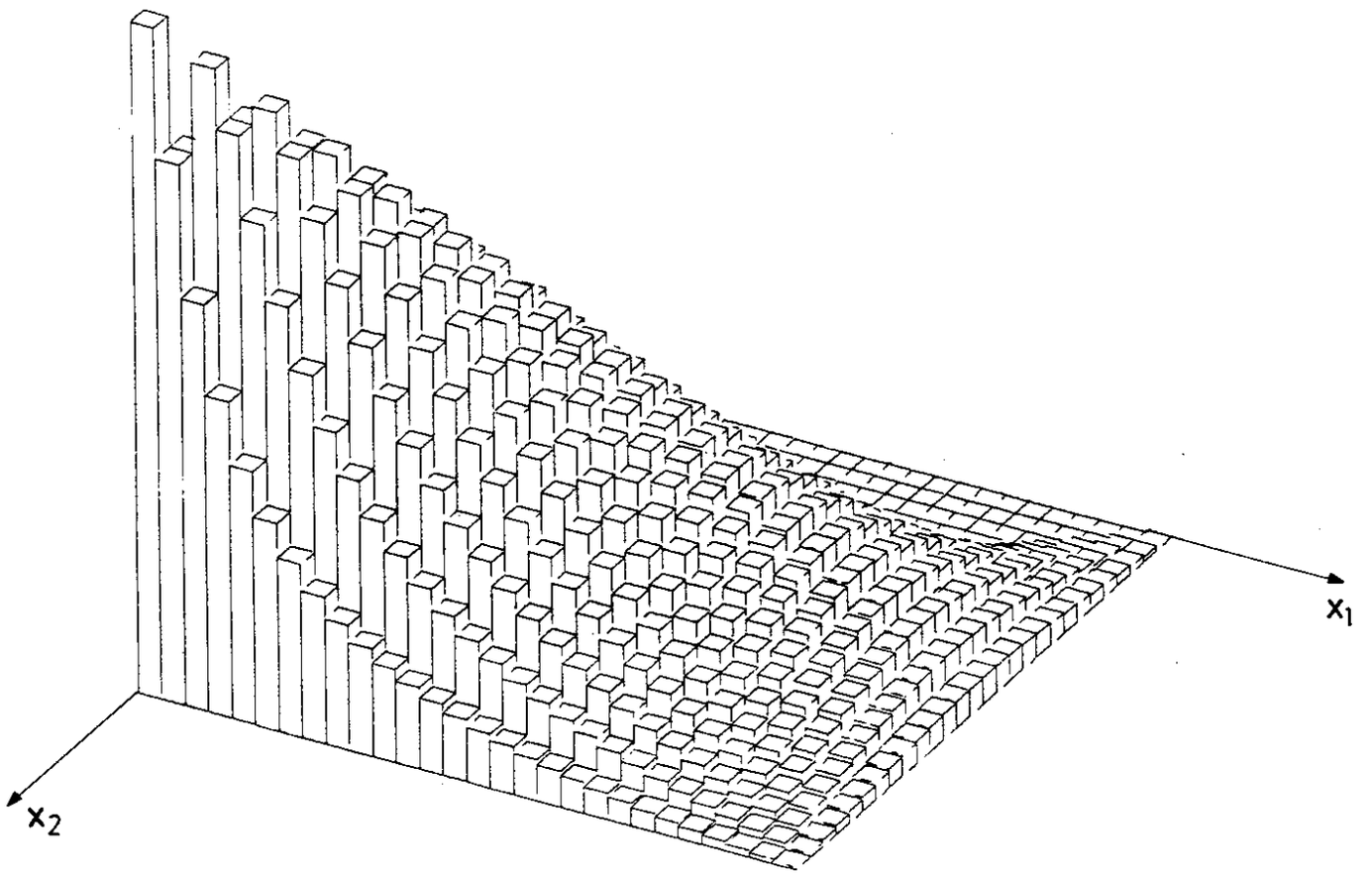


Fig.11b

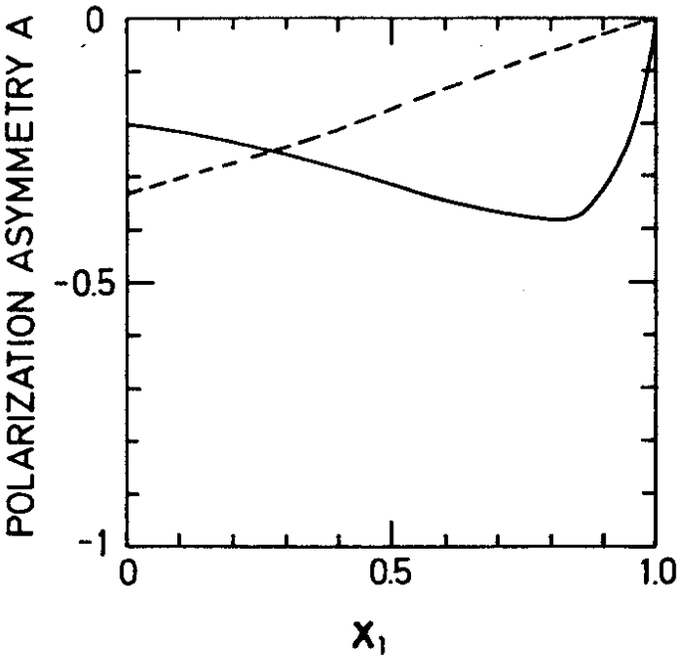


Fig.12

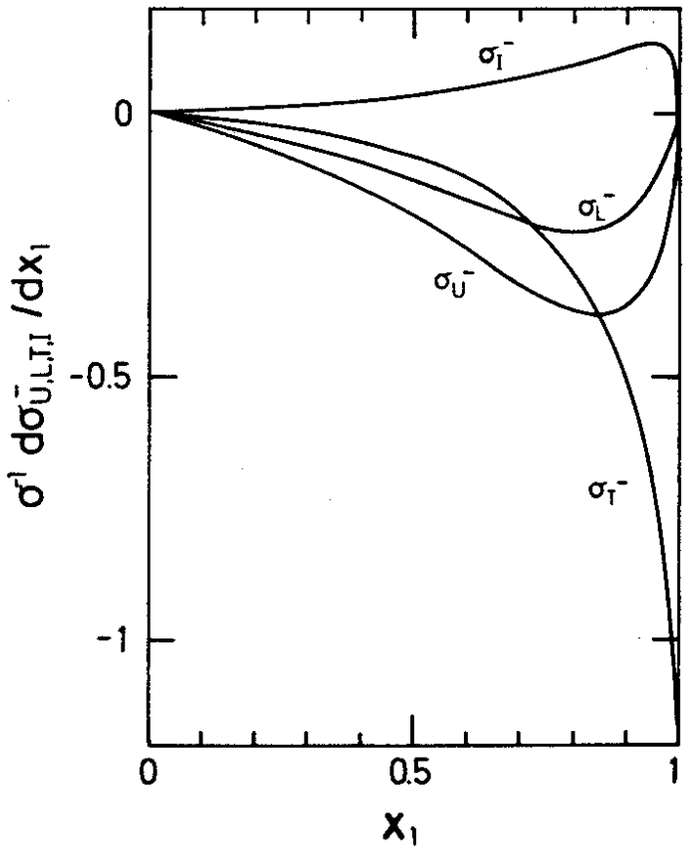


Fig.13a

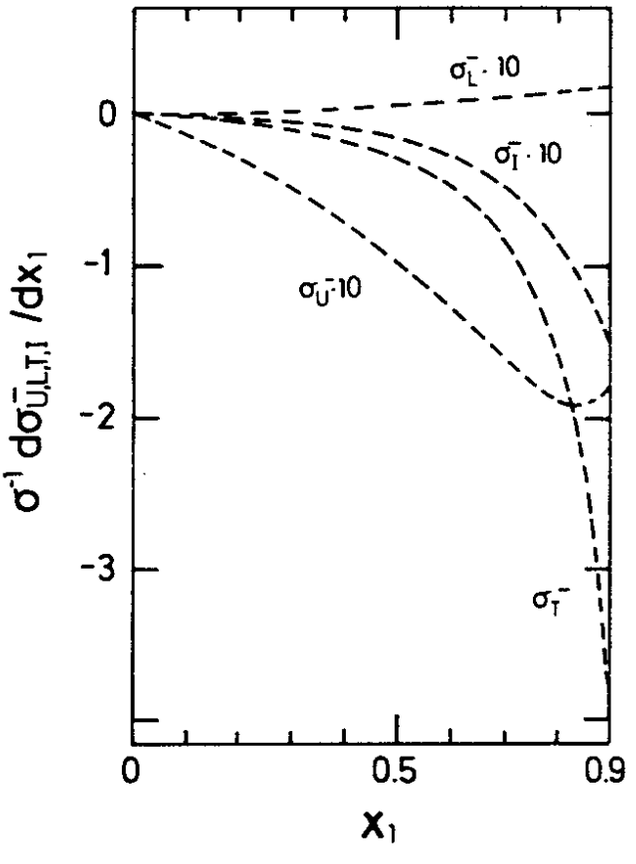


Fig.13b

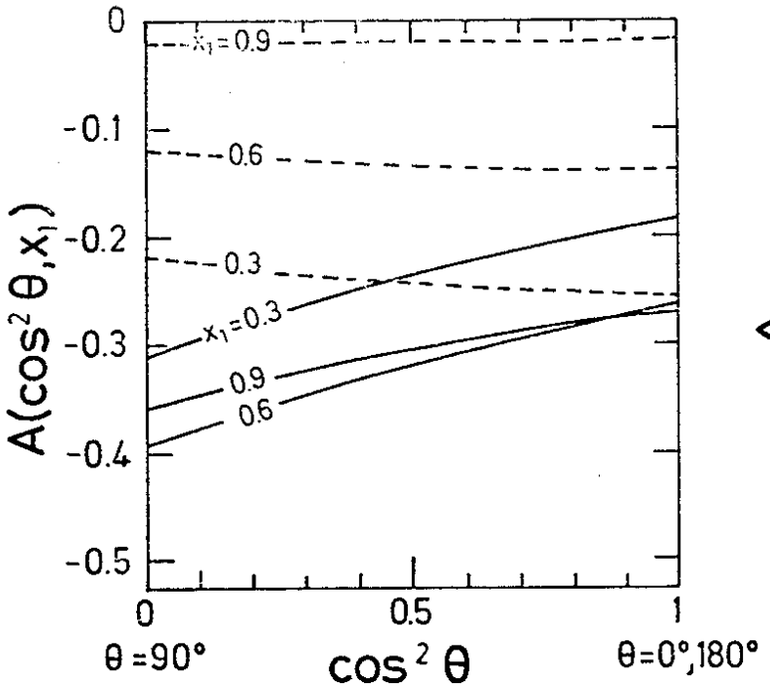
0
-0.1
-0.2
-0.3
-0.4
-0.5
$A(\cos^2\theta, x_1)$
$x_1=0.9$
0.6
0.3
$x_1=0.3$
0.9
0.6
0
0.5
1
θ =90°
$\cos^2\theta$
θ=0°,180°

Fig.14

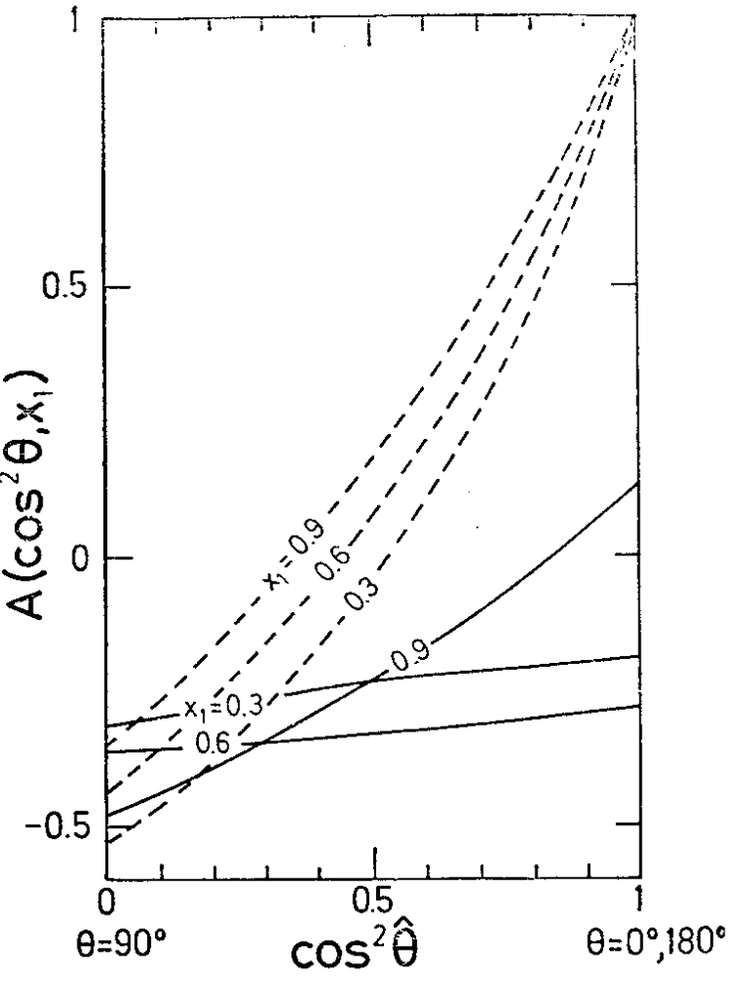
1
0.5
0
-0.5
$A(\cos^2\hat{\theta}, x_1)$
$x_1=0.9$
0.6
0.3
0.9
$x_1=0.3$
0.6
0
0.5
1
θ=90°
$\cos^2\hat{\theta}$
θ=0°,180°

Fig.15